Journal Pre-proof

Elaborated study of Cu(II) carbosilane metallodendrimers bearing substituted iminopyridine moieties as antitumor agents

Riccardo Carloni, Natalia Sanz del Olmo, Barbara Canonico, Mariele Montanari, Caterina Ciacci, Gianluca Ambrosi, F. Javier de la Mata, Maria Francesca Ottaviani, Sandra García-Gallego

PII: S0223-5234(21)00141-0

DOI: https://doi.org/10.1016/j.ejmech.2021.113292

Reference: EJMECH 113292

To appear in: *European Journal of Medicinal Chemistry*

Received Date: 5 December 2020

Revised Date: 7 February 2021

Accepted Date: 8 February 2021

Please cite this article as: R. Carloni, N. Sanz del Olmo, B. Canonico, M. Montanari, C. Ciacci, G. Ambrosi, F. Javier de la Mata, M.F. Ottaviani, S. García-Gallego, Elaborated study of Cu(II) carbosilane metallodendrimers bearing substituted iminopyridine moieties as antitumor agents, *European Journal of Medicinal Chemistry*, https://doi.org/10.1016/j.ejmech.2021.113292.

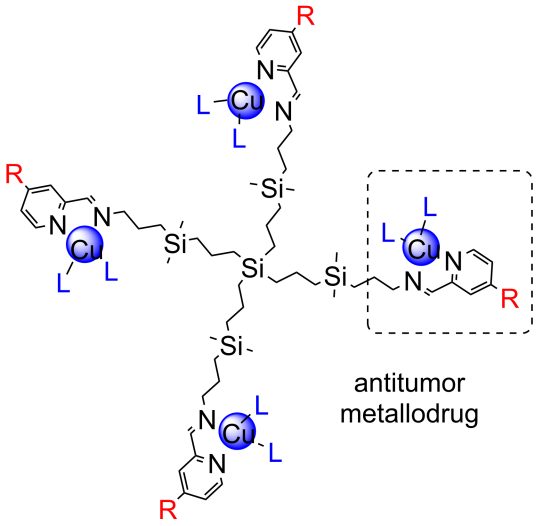

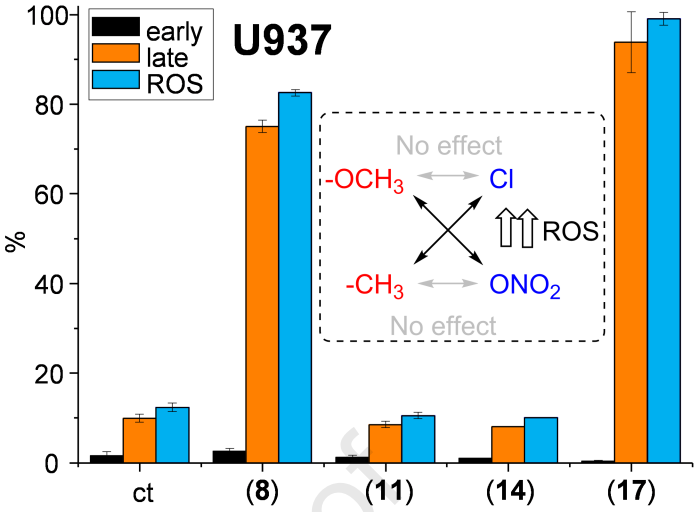

Elaborated study of Cu(II) carbosilane metallodendrimers bearing substituted iminopyridine moieties as antitumor agents

Riccardo Carloni [1], Natalia Sanz del Olmo [2], Barbara Canonico [3], Mariele Montanari [3], Caterina Ciacci [3], Gianluca Ambrosi [1], F. Javier de la Mata [2,4,5*], Maria Francesca Ottaviani [1*], and Sandra García-Gallego [2,4,5*]

[1] Department of Pure and Applied Sciences, University of Urbino "Carlo Bo", 61029, Urbino, Italy
[2] Department of Organic and Inorganic Chemistry, and Research Institute in Chemistry "Andrés M. del Río" (IQAR), University of Alcalá, 28805, Madrid, Spain
[3] Department of Biomolecular Science (DiSB), University of Urbino "Carlo Bo", Urbino 61029, Italy
[4] Networking Research Center on Bioengineering, Biomaterials and Nanomedicine (CIBER-BBN), 28029, Madrid, Spain
[5] Institute Ramón y Cajal for Health Research (IRYCIS), 28034, Madrid, Spain
* Correspondence: sandra.garciagallego@uah.es, javier.delamata@uah.es, maria.ottaviani@uniurb.it

Abstract: Iminopyridine-decorated carbosilane metallodendrimers have recently emerged as a promising strategy in the treatment of cancer diseases. Their unique features such as the nanometric size, the multivalent nature and the structural perfection offer an extraordinary platform to explore structure-to-property relationships. Herein, we showcase the outstanding impact on the antitumor activity of a parameter not explored before: the iminopyridine substituents in *meta* position. New Cu(II) carbosilane metallodendrimers, bearing methyl or methoxy substituents in the pyridine ring, were synthesized and thoroughly characterized. Electron paramagnetic resonance (EPR) was exploited to unveil the properties of the metallodendrimers. This study confirmed the presence of different coordination modes of the Cu(II) ion (Cu-N_2O_2, Cu-N_4 and Cu-O_4), whose ratios were determined by the structural features of the dendritic molecules. These metallodendrimers exhibited IC_{50} values in the low micromolar range (< 6 μM) in tumor cell lines such as HeLa and MCF-7. The subsequent *in vitro* assays on both healthy (PBMC) and tumor (U937) myeloid cells revealed two key facts which improved the cytotoxicity and selectivity of the metallodrug: First, maximizing the Cu-N_2O_2 coordination mode; second, adequately selecting the pair ring-substituent/metal-counterion. The most promising candidates - $G_1(\text{-}CH_3)Cl$ **(8)** and $G_1(\text{-}OCH_3)NO_3$ **(17)**, exhibited a substantial increase in the antitumor activity in U937 tumor cells, compared to the non-substituted counterparts, probably through two different ROS-production pathways.

Keywords: metallodendrimers; pyridine; electron paramagnetic resonance; copper; cancer.

1. Introduction

Although cancer death rate is falling since 1991, it is still a major threat to public health [1]. While early detected forms of the disease are easier to deal with, metastasis is the primary cause of cancer morbidity and mortality [2]. This led to the development of unspecific therapies, directed to the whole body, bearing the huge burden of dealing with differentiated cell types and tissues. Nowadays, the need for a smart treatment, capable of selectively targeting tumor cells is more than ever needed to overcome traditional drugs' limitations.

Nanoparticles are emerging in numerous branches of science as a revolutionary approach to long known problems. In biomedicine, they have been exploited for many clinical applications, like drug carriers, genetic material delivery to tumors, cancer diagnostic, imaging contrast agents and more [3, 4]. The reason for this success is their nanometric size, responsible for the enhanced permeability retention effect in solid tumors, and the presence of multiple groups in their surface, available for modifications to adapt to the most diverse environment. Dendrimers are a particular class of nanoparticles which rose a lot of hype in the scientific community due to their high potential in the biomedical field. This class of starburst-shaped, highly branched

polymers features marked monodispersity and represents the ideal candidate to develop a library of anticancer drugs. Their properties are dictated not only by the peripheral groups, but also by the nature of their scaffold: poly(amidoamine) (PAMAM), poly(propyleneimine) (PPI), phosphorhydrazone (PPH) and carbosilane (CBS) are among the most common dendritic molecules.

The combination of organic ligands and metals proved to be one of the most efficient pathways to deal with tumors, with cisplatin rapidly making its way to become the golden standard for many cancer forms, often in combination with radiotherapy [5]. Its high toxicity and induced resistance, though, pose limits to the long-term use of this metallodrug [6]. Alternative transition metal complexes have been reported, bearing nickel(II), cobalt(II), copper(II), ruthenium(III), and ruthenium(IV). Their cytotoxicity is mainly associated to apoptosis, autophagy, DNA damage, and/or cell cycle inhibition [7]. Metallodendrimers, defined as the combination of dendritic skeletons and metal ions, have recently proved to be very potent in anticancer *in vitro* and *in vivo* assays. They often exhibit low IC_{50} values and high selectivity, thus decreasing the side effects [8]. In recent articles, we explored the potential of Cu(II) and Ru(II)-conjugated carbosilane metallodendrimers, where the metal ions are chelated *via* polydentate *N,N*-donor iminopyridine ligands, placed on the periphery of the dendrimer branches. The carbon-silicon pattern of the skeleton grants high flexibility, stability and improves the interaction with the cell membranes, while metal ions are largely responsible for the antitumor mechanism, triggering a mixed mechanism of ROS formation and apoptosis [9, 10].

With the aim of unfolding more features of the structure-activity relationship (SAR) of this class of molecules, we explored the effects of the iminopyridine ring decoration, both under a physicochemical and a biological point of view. A careful selection of both the position and nature of the substituent was performed, based on previous results in the literature [11]. For example, no electron-withdrawing substituent was chosen, since it proved to diminish the anticancer activity [12]. Furthermore, stronger effects on the pyridine nitrogen are produced by substituents on *para* position [13]. The pyridine ring was therefore substituted on position 4 with a methyl or methoxy function. On the basis of previous studies, two different Cu(II) counterions were chosen: chloride, which proved to augment the antitumor potency, and nitrate, which improves the physicochemical properties of the molecule, including the solubility in water [14]. Computer-aided Electron Paramagnetic Resonance (EPR) was exploited to characterize the paramagnetic metal complexes, and meaningful information was extracted regarding the effect of generation, ring substituent, and counterion, setting the best route for the following biological assays.

2. Results and Discussion

2.1 Synthesis of carbosilane dendrimers bearing substituted iminopyridine moieties and derived Cu(II)-metallodendrimers

Inspired by our previous work on iminopyridine carbosilane dendrimers [15], two new families bearing methyl and methoxy substituents on the iminopyridine rings were synthesized. The general formula G_n-[NCPh(*m*-R)(*o*-N)]$_m$ indicates the dendrimer generation (n = 0, 1, 2), the number of terminal groups (m = 1, 4, 8) and the ring substituent in *meta* position (R = Me, OMe). For the metallodendrimers, a simplified nomenclature will be employed throughout the text, which clearly highlights the main structural differences: G_n-RL, where n indicates the dendrimer generation (n= 0, 1, 2), R the ring substituent (R = Me, OMe) and L is the copper counterion (L = Cl, NO_3). Non-dendritic G_0 compounds will be referred as mononuclear ligands and metal complexes. **Scheme 1** shows the synthetic route adopted in this work. The carbosilane dendrimers G_n-[NH_2]$_m$ (n=0, m=1 (**I**), n=1, m=4 (**II**), n=2, m=4 (**III**))[16] react *via* Schiff-base condensation with two different aldehydes (2-Formyl-4-picoline and 4-Methoxy-2-pyridinecarbaldehyde), leading to the formation of the corresponding dendrimers with terminal R-substituted iminopyridine ligands. All reactions were carried out under inert atmosphere and in the presence of $MgSO_4$ for water removal. The resulting yellowish (**1-3**) and amber (**1-6**) compounds were isolated as oily products and kept under inert atmosphere to prevent degradation.

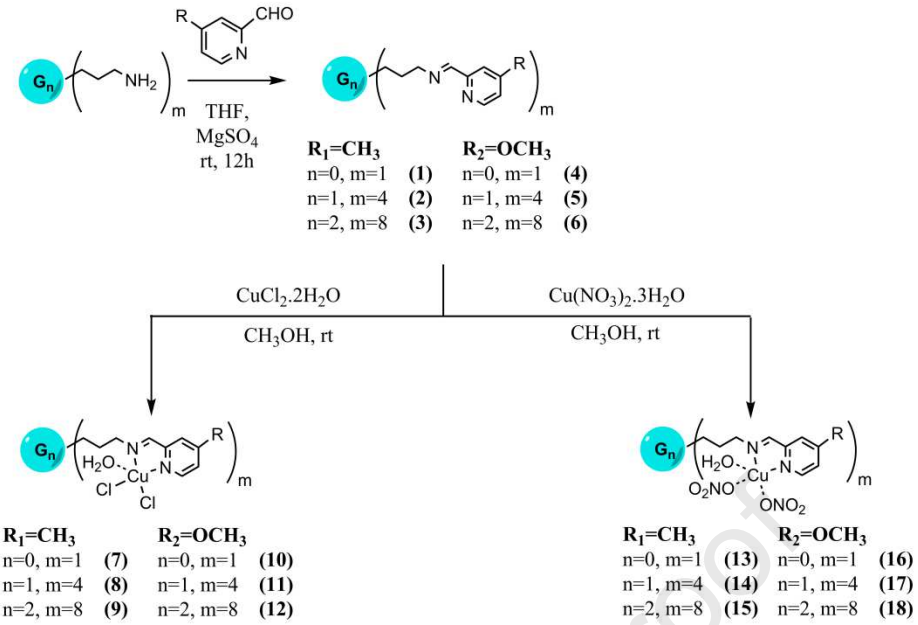

Scheme 1. Synthetic route towards carbosilane dendrimers (**1-6**) and Cu(II)-metallodendrimers (**7-18**) featuring R-substituted iminopyridine ligands.

The structural characterization of dendrimers **1-6** through elemental analysis, mono- and bidimensional NMR spectroscopy and mass spectroscopy confirmed the formation of the desired species (**Figures S1-S24**). Compared to the precursor dendrimers, the most relevant changes in the NMR spectra arise from the formation of the imine bond. As example, **Table 1** summarizes the shifts in selected ^{1}H-NMR signals for first generation precursors and iminopyridine dendrimers. The imine proton –CH=N- appears at ~ δ 8.30 ppm in the ^{1}H-NMR spectra, while it is observed in the range 150.7-156.5 ppm in ^{13}C-NMR spectra. The methylene group directly connected to the imine bond –CH_2N- was shifted from 2.63 ppm in the precursors to ~ δ 3.60 ppm, while the following groups also undergo a shift, but with low intensity. The rest of signals from the carbosilane scaffold appear at similar chemical shifts to those of their precursors [16]. The signals from the aromatic rings appear at the expected values. In ^{1}H-NMR spectra, they arise in the range δ 7.08-8.48 ppm for methyl-compounds **1**-**3** and in δ 6.80-8.43 ppm for methoxo-compounds **4**-**6**, clearly observing the influence of the substituent in *meta* position to the iminopyridine moiety. Furthermore, a singlet is found at ~ δ 2.35 ppm or at ~ δ 3.85 ppm, from the –CH_3 or the –OCH_3 moieties, respectively. Bidimensional spectra were recorded for an accurate assignment of the signals. **Figure 1** depicts the (^{1}H-^{13}C)-gHSQC spectra for dendrimer **5**, as selected example, as well as its ESI-TOF spectrum identifying the molecular peak. Unfortunately, mass spectra did not provide information about higher-generation dendrimers.

Table 1. ^{1}H-NMR shifts for selected signals in the first-generation precursor **II** and the resultant iminopyridine dendrimers **2** (R = Me), **5** (R = OMe) and **X** (R = H).

Dendritic fragment		**δ (ppm)**			
		II[a]	**2**	**5**	**X**[b]
-Si(CH$_2$)$_3$N-	-SiC*H*$_2$-	0.44-0.54	0.52	0.52	0.53
	-C*H*$_2$-	1.34	1.68	1.67	1.70
	-C*H*$_2$N	2.63	3.62	3.61	3.64
-N=CH-		-	8.32	8.29	8.35
R-Py	*o*-,[c]	-	7.79	7.47	7.72
	m-,[c]	-	8.48	8.39	8.63
	p-,[c]	-	7.10	6.80	7.29
	R	-	Me, 2.36	OMe, 3.85	H, 7.98

[a]Previously reported data [16]; [b]previously reported data [15]; [c] position to imine moiety.

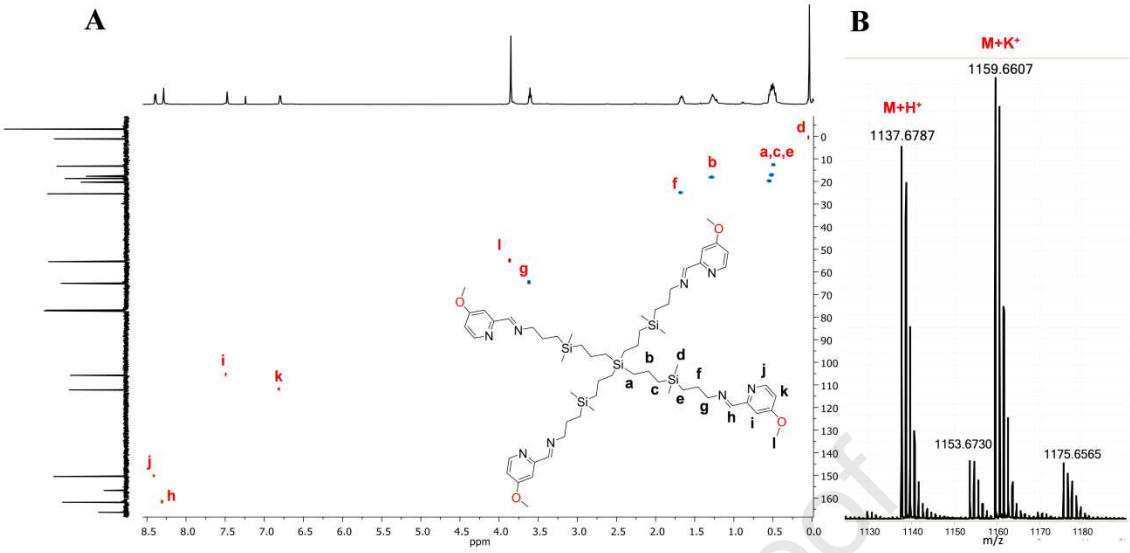

Figure 1. Characterization of first-generation dendrimer **5**, as selected example. A) (^{1}H-^{13}C)-gHSQC spectrum (500MHz, $CDCl_3$). B) ESI-TOF spectrum (calculated *m*/*z* for M = 1136.67).

Dendrimers G_n-[NCPh(*m*-CH_3)(*o*-N)]$_m$ (**1-3**) and G_n-[NCPh(*m*-OCH_3)(*o*-N)]$_m$ (**4-6**) are decorated with bidentate ligands featuring two nitrogen donor atoms, exploited to coordinate Cu(II) in the next step. Dendrimers **1-6** reacted with solutions of $CuCl_2{\cdot}2H_2O$ or $Cu(NO_3)_2{\cdot}3H_2O$ in methanol, in a 1:1 branch-Cu(II) ratio. The fast coordination leads to the formation of the final products, isolated as green solids (**7**-**18)**. A substantial improvement from the previous protocol [14, 17] is the exchange of DMF to MeOH as reaction solvent, which simplifies the isolation of the final products. Elemental analysis and FTIR of the different solid samples confirms the formation of the desired metal complexes and metallodendrimers. Their behavior in solution was subsequently studied through EPR (section 2.2), considering the paramagnetic nature of Cu(II) which hinders an accurate NMR characterization. Nevertheless, an additional study to confirm the metal coordination was performed, where Cu(II) was replaced by Zn(II). In this case, after the metal coordination, both NMR and FTIR spectra showed a consistent de-shielding of the signals with respect to the free ligand, confirming the coordination of the metal (**Figure S25**). Given the similarities between Cu(II) and Zn(II) ions, we assumed that this was the case for Cu(II) as well, as later confirmed by EPR analysis. While G_0 complexes are fully soluble in water, G_1 and G_2 counterparts require the addition of a small portion of DMSO (1%) for a total dissolution. Compared to their unsubstituted iminopyridine analogues, the presence of the methyl or methoxy substituent decreases their solubility, even for the nitrate complexes which were easily dissolved in water [14].

A small yet visible discrepancy between the calculated and experimental elemental analysis of G_0 compounds brought the attention to the possible formation of ML_2 species during the metal coordination. The mass spectra and EPR analysis of these compounds confirmed such hypothesis. In solid state, G_0 complexes revealed a small fraction of ML_2 species, bearing four nitrogen sites coordinating one Cu(II) ion. In solution, though, EPR demonstrated that the ML_2 species are clearly predominant (see section 2.2). In order to gain further insight in this reaction, additional experiments were performed using 2:1 ligand:Cu(II) reaction conditions. Independently of the Cu(II) salt used, ligands **1** and **4** led to the formation of ML_2 complexes, with a proposed structure of [G_0-[NCPh(*m*-CH_3)(*o*-N)]$_2$Cu·H_2O] (**7***) and [G_0-[NCPh(*m*-OCH_3)(*o*-N)]$_2$Cu·H_2O] (**10***). Selected samples were then studied through EPR, as explained in section 2.2. Comparing our data with bibliography, the analogous complex G_0-[NCPh(*o*-N)$CuCl_2{\cdot}H_2O$], bearing an H in *meta* position, had shown accurate agreement of experimental and theoretical elemental analysis values (<2.5% deviation), while mass spectra provided no conclusive results about the metal complex structure [17]. It has been reported that the presence of the Me and MeO substituents in pyridine rings increases the basicity of the nitrogen atom. In our case, this leads to a favourable CuN_4 coordination, as later confirmed by EPR studies. The presence of *N,O*-fenolimine ligands also favours the formation of ML_2 species, such as the complex [G_0-[NCPh(*o*-O)]$_2$Cu·H_2O] previously described [17].

Fortunately, the formation of ML_2 species was not observed for generation 1 and 2 metallodendrimers. Elemental analyses indicate the exclusive formation of mononuclear complexes, highlighting their high monodispersity. These results are in agreement with those obtained with the non-substituted counterparts

G_1-[NCPh(*o*-N)]$_4$ and G_2-[NCPh(*o*-N)]$_8$ [17]. In this study, Cu(II) was added at increasing concentrations to the dendrimers. We found that Cu-N_4 coordination was only stabilized at low Cu(II) concentrations for G_1 and G_2 dendrimers, while at stoichiometric ratios no ML_2 species were observed. Nevertheless, as later explained in EPR section, the presence of the methyl and methoxy functions seems to induce the Cu-N_4 coordination in solution, and this effect decreases with the increase in generation.

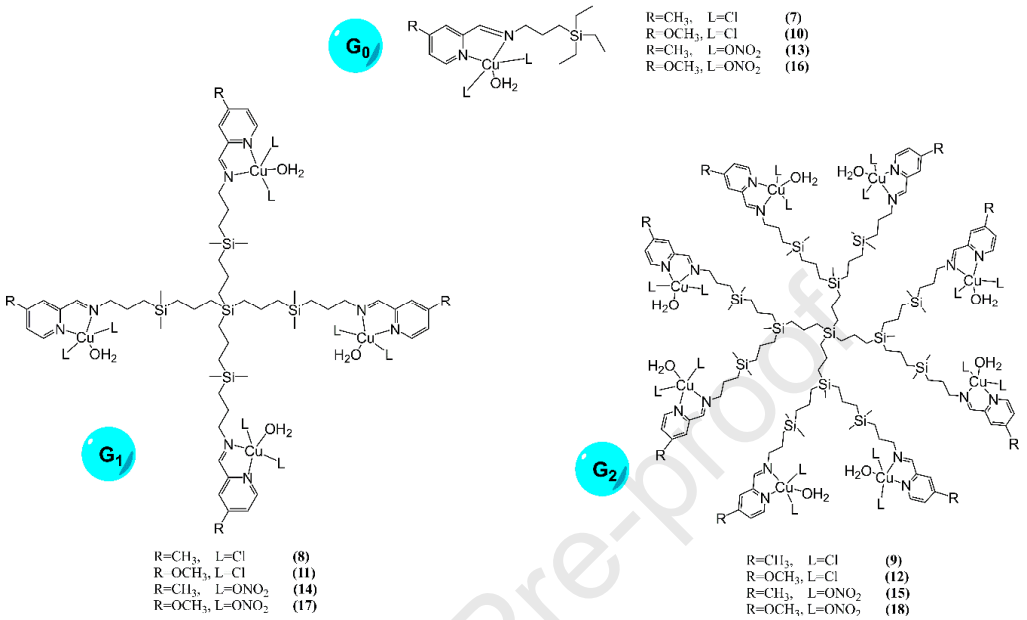

Figure 2. Proposed structures in solid state for Cu(II) carbosilane metallodendrimers synthetized in this work.

2.2 Electron Paramagnetic Resonance Analysis

EPR is a valuable tool in the characterization of paramagnetic metal complexes, providing a tridimensional picture of the molecule surroundings. In this work, it proved particularly useful in establishing the Cu(II) coordination and geometry. Complexes **7**-**18** were dissolved in a water solution containing 3% DMSO at two different concentrations: 1 mM and 0.5 mM. Samples were tested after 15 minutes of equilibration. The experimental spectra were then computed to extract structural and dynamical parameters, as described in the Materials and Methods section [18].

Generation 0 complexes **7**, **10**, **13** and **16** revealed a surprising behavior. **Figure 3A** shows, as selected example, the experimental (black line) and the computed (red line) EPR spectra of G_0(-OCH_3)Cl **(10)** at 1 mM. The computation was performed using the main magnetic g_{ii} and A_{ii} components – g_{xx} = 2.001, g_{yy} = 2.102, g_{zz} = 2.375; A_{xx} = 5 G, A_{yy} = 5 G, A_{zz} = 236 G. The magnetic g_{ii} and A_{ii} components provide information about the structure and geometry of the Cu(II) complexes by comparing with similar parameters obtained in the literature [14, 19-23]. On this basis, these components were characteristic of a Cu(II) coordination with 4 nitrogen sites (Cu-N_4 coordination) in a distorted square planar geometry, accomplished through the formation of ML_2 species. Furthermore, the line shape of the spectra did not change by diluting sample from 1 mM to 0.5 mM, suggesting a high stability of the ML_2 complexes. In this respect, it is useful to underline that Cu(II) ions preferentially interact with 4 nitrogen sites if they are geometrically and sterically available. The computation procedure allowed us to also evaluate the correlation time for motion, τ, which provides a measure of the Cu(II) complex mobility: higher τ, lower the mobility. The Cu-N_4 complex shows a high mobility (τ = 33 ps), related to the small size of the generation 0 complexes.

The situation completely changed for first and second generation metallodendrimers. The experimental spectrum of G_1(-OCH_3)Cl (**11)** at 1 mM is shown in **Figure 3B** (black line). The main component of this spectrum was computed as shown in the figure (red line). The magnetic parameters g_{ii} and A_{ii} used for the computation were g_{xx} = 2.002, g_{yy} = 2.102, g_{zz} = 2.470; A_{xx} = 5 G, A_{yy} = 5 G, A_{zz} = 172 G. For square planar structures (zz components > xx and yy components), the increase in g_{ii} (mainly g_{zz}) and decrease in A_{ii} (mainly A_{zz}), corresponding to an increase in the g_{ii}/A_{ii} ration, reflects a decreased number of complexes nitrogen sites and, consequently, a less homogeneous complex structure. Therefore the g_{ii} and A_{ii} components, again on the basis

of the previous studies [14, 19-23], are characteristic of a square planar (distorted, as the discrepancy between g_{xx} and g_{yy} indicates) Cu-N_2O_2 coordination. This coordination was expected for Cu(II) chelated through two nitrogen sites from a dendrimer branch, while the two other coordinating sites of a distorted square planar structure were probably water molecules hydrating the Cl^- ions in vicinity of the Cu(II) ions. In this case, since the ions coordinated only one dendrimer branch, the ions were more mobile and the correlation time for motion, τ, decreased from 33 ps in G_0(-OCH_3)Cl **(10)** (**Fig. 3A**) to 17 ps in G_1(-OCH_3)Cl (**11**) (**Fig. 3B**). Interestingly, as indicated by arrows in **Fig. 3B**, other two components slightly contributed to the EPR spectrum: a second component attributed to the Cu-N_4 coordination, meaning that a small fraction of ions was still able to coordinate two dendrimer branches; and a third component, due to Cu(II) ions in water (Cu-O_4 coordination). Therefore, a small fraction of ions, after saturating the nitrogen sites, were sitting outside the dendrimers in the external water solution. This component was computed as shown in **Figure 3C**. It is interesting to note here that G_1(-CH_3)Cl (**8**) showed the highest intensity of the EPR spectrum among all dendrimers, in line with a weakening of the electrostatic binding with the Cl^- counter-ion.

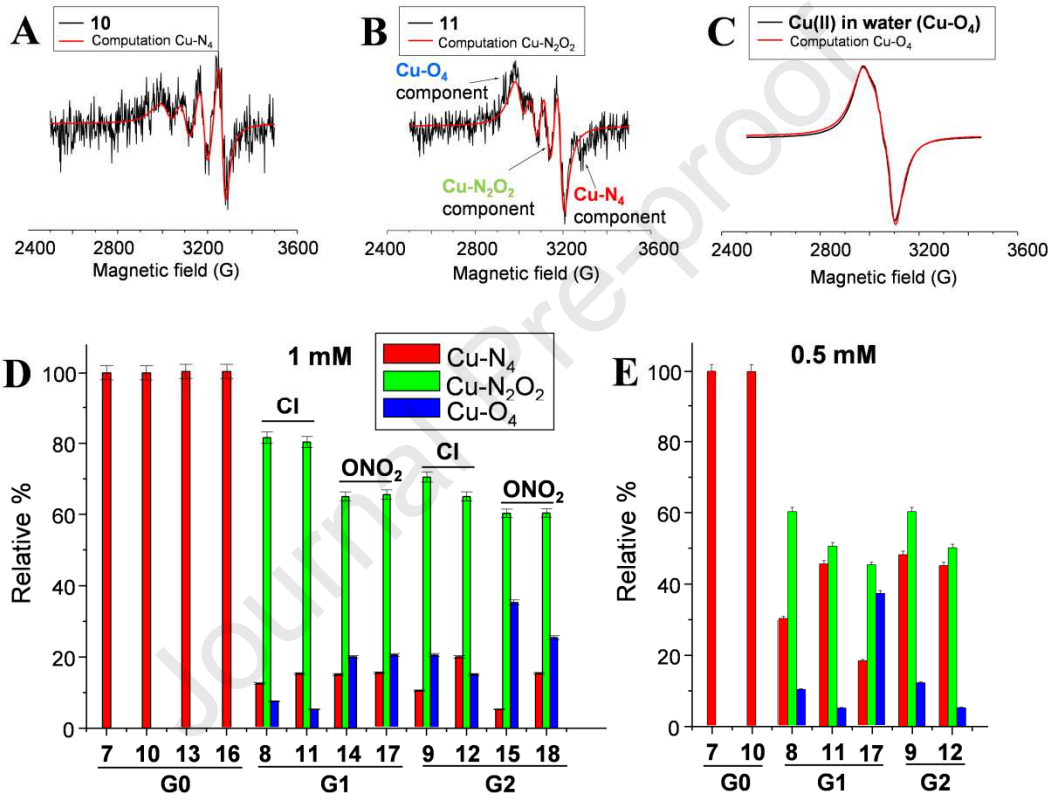

Figure 3. (A) Experimental (black line) and computed (red line - Cu-N_4 component) EPR spectra of G_0(-OCH_3)Cl **(10)** at 1 mM concentration. (B) Experimental (black line) and computed (red line, Cu-N_2O_2 component) of G_1(-OCH_3)Cl (**11**) at 1 mM concentration. (C) Experimental (black line) and computed (red line) EPR spectra of Cu(II) in water (Cu-O_4 component). (D/E) Relative percentages of the three components (Cu-N_4, Cu-N_2O_2, Cu-O_4) in EPR spectra for the various samples at 1 mM (D) and 0.5 mM (E). Nitrate complexes at 0.5 mM are not shown due to the noisy spectra (except for **17**).

Other examples of informative EPR spectra are shown in the Supporting Information (**Figure S26**). The same three spectral components (arising from Cu-N_4, Cu-N_2O_2, and Cu-O_4 coordination) constituted the different spectra of the various samples (generation 0, 1 and 2 dendrimers at concentrations 1 and 0.5 mM), but at different relative percentages. **Figures 3D** and **3E** show the relative percentages of these three components for the various samples. These percentages were obtained by subtracting the computed components in **Fig. 3A-C** from the overall spectra at the needed extents, and double integrating both the components and the overall spectra. Relevant information can be extracted from **Figures 3D** and **3E**, which may be summarized as follows:

Cu-N_4 was the only component present for zero generation complexes G_0(-CH_3)Cl **(7),** G_0(-OCH_3)Cl **(10)**, G_0(-CH_3)NO_3 **(13)** and G_0(-OCH_3)NO_3 **(16)**, at both 1 mM and 0.5 mM. This confirms that, in solution, these complexes form ML_2 species with high stability. Surprisingly, when ML_2 complexes are synthesized on purpose, as G_0(-OCH_3)$_2$ (**10***) selected as example (**Figure S27**), Cu-N_4 destabilized and the Cu-N_2O_2

coordination prevailed, probably due to ligand aggregation that impeded dendrimer-dimers formation. Self-aggregation of the ligands at high concentration is probable, due to their surfactant nature (hydrophobic core and hydrophilic surface).

For first generation metallodendrimers $G_1(-CH_3)Cl$ **(8),** $G_1(-OCH_3)Cl$ **(11)**, $G_1(-CH_3)NO_3$ **(14)** and $G_1(-OCH_3)NO_3$ **(17)**, at a concentration 1 mM, the relative amount of Cu-N_4 significantly decreased, if compared to the corresponding G_0 cases, in favor of the Cu-N_2O_2 component. This is probably due to unfavorable formation of ML_2 species for higher generation dendrimers, being difficult for the ions to coordinate two dendrimer branches. The ion-ion repulsion at the dendrimer surface provoked a fraction of ions to be extruded by the nitrogen sites and be confined externally to the dendrimer surface, forming the Cu-O_4 component. The relative percentage of the Cu-O_4 component was small but increased from chloride to nitrate counter-ion, showing a lower stability of the Cu(II)-dendrimer complexes in presence of the nitrate counter-ion, if compared to the chloride one. This is in line with previous results [14]. By diluting the samples from 1 to 0.5 mM, the Cu-N_4 component increased again with respect to the Cu-N_2O_2, since ion-ion repulsion decreased, and the dendrimer branches better approached to each other to let Cu(II) coordinating with 4 nitrogen sites. The results for the nitrate derivative $G_1(-CH_3)NO_3$ **(14)** at 0.5 mM are not shown, because the spectra were very noisy, even after 20 scans (all spectra were recorded in the same instrumentation conditions for a matter of comparison and the experiment was repeated after 24 h to verify the stability of the system over time into the one-day time range). This finding further indicates a decrease in stability of the Cu(II)-dendrimers complexes when the nitrate counter-ion substituted the chloride one. However, surprisingly, $G_1(-OCH_3)NO_3$ **(17)** showed a quite high intensity also at a concentration of 0.5 mM, probably due to the effect of the methoxy group that increased its solubility. The spectra of **17** clearly showed a significant increase of the Cu-O_4 relative percentage, indicating a perturbative effect of the nitrate counter-ion that prevents the ions to approach the nitrogen sites.

For $G_2(-CH_3)Cl$ **(9)** and $G_2(-OCH_3)Cl$ **(12)** and at a concentration 1 mM, a steric hindrance provoked by the increased density of surface groups, partially impeded the Cu(II) coordination with the nitrogen sites. As a consequence, the Cu-O_4 component increased its relative percentage, mainly at the expenses of Cu-N_2O_2 (the ions exchanged at the external surface). Therefore, second generation dendrimers formed less stable Cu-N_2O_2 complexes, if compared to the first generation dendrimers. Similarly to first generation complexes, at 0.5 mM the Cu-N_4 component substantially increased due to the proximity of dendritic branches.

Finally, for G_1 metallodendrimers at 1 mM, we observed a similar influence of methyl and methoxy substituents but a different effect of the counterion (see **8** vs **11** and **14** vs **17**). However, at lower concentrations, or for G_2 complexes, the effect of the substituent was clearly visible: the -CH_3 function seemed to perturb (or, at least, not favor) the Cu-N_4 complexation if compared to the -OCH_3 function, thus decreasing the formation of ML_2 species. The predominant resonance effect in the methoxy function produces an increased basicity in the pyridine nitrogen, which favors the coordination of Cu(II) with 4-nitrogen sites. In our former studies [17], ML_2 species such as [G_0-[NCPh(*o*-O)]$_2$Cu·H_2O] exhibited a lower antitumor activity, compared to similar ML complexes such as G_0-[NCPh(*o*-N)$CuCl_2$·H_2O]. On this basis, we concluded that the most promising metallodendrimers should minimize the Cu-N_4 coordination in favour of Cu-N_2O_2 complexes, potentially higher interacting species. The most prominent and stable Cu-N_2O_2 complex was formed for $G_1(-CH_3)Cl$ **(8)**, among chloride compounds, and $G_1(-OCH_3)NO_3$ **(17)**, among nitrate ones. Therefore, we also expect a good biological activity for these metallodendrimers.

2.3 Biological assays

The metallodendrimers herein described gather all necessary properties to be tested as potential antitumor drugs: stability and solubility in water solutions. Subsequently, G_1 and G_2 metallodendrimers were evaluated in a series of *in vitro* assays to study their cytotoxic and cytostatic effect in tumor and healthy cells, as well as the impact on intracellular organelles such as lysosomes, mitochondria and autophagic vacuoles. G_0 complexes were excluded from these studies, considering their tendency to preferentially form ML_2 species in solution.

2.3.1 *In vitro* cytotoxicity in HeLa and MCF-7 tumor cell lines

In order to evaluate the cytotoxicity of the new family of copper (II) metallodendrimers, MTT assays were performed in HeLa and MCF-7 tumor cell lines. This preliminary study allowed us to compare the results with those obtained for analogous Cu(II) metallodendrimers bearing unsubstituted iminopyridine moieties [14].

Table 2 summarizes the experimental IC_{50} values obtained after 24 h treatment of the cells with G_1 and G_2 metallodendrimers, comprising 4 and 8 Cu(II) complexes respectively.

Table 2. Cell viability expressed as IC_{50} (half maximal inhibitory concentration) in two tumor cell lines (HeLa and MCF-7) after 24 h treatment with the new families of Cu(II) metallodendrimers.

Compound	Cu(II) atoms	IC_{50} ± SD (μM) HeLa	MCF-7
$G_1(\text{-}CH_3)Cl$ **(8)**	4	1.9 ± 0.5	2.7 ± 0.6
$G_2(\text{-}CH_3)Cl$ **(9)**	8	3.0 ± 0.4	2.7 ± 0.0
$G_1(\text{-}OCH_3)Cl$ **(11)**	4	2.2 ± 0.0	3.2 ± 0.3
$G_2(\text{-}OCH_3)Cl$ **(12)**	8	2.9 ± 0.1	3.4 ± 0.6
$G_1(\text{-}CH_3)NO_3$ **(14)**	4	2.6 ± 0.2	2.3 ± 0.0
$G_2(\text{-}CH_3)NO_3$ **(15)**	8	1.9 ± 0.6	5.1 ± 2.4
$G_1(\text{-}OCH_3)NO_3$ **(17)**	4	2.3 ± 0.2	2.7 ± 0.5
$G_2(\text{-}OCH_3)NO_3$ **(18)**	8	2.4 ± 0.2	5.6 ± 0.0

The new metallodendrimers showed a potent antitumor activity in both cell lines, with IC_{50} values in the low micromolar range (1.9-5.6 μM). These values are below the reported range of cisplatin, which exhibited IC_{50} values of 19.40±1.85 and 22.38±0.62 μM in HeLa and MCF-7 cells, respectively [24]. No clear trends were observed regarding the dendrimer generation, the nature of the iminopyridine substituent or the type of metal counter-ion. Nevertheless, a general improvement in the anticancer activity for all metallodendrimers is found, compared to those previously reported with the pyridine fragment (without substituent) [14]. For example, $G_1(\text{-}CH_3)Cl$ **(8)** and $G_1(\text{-}OCH_3)Cl$ **(11)** show IC_{50} values around 2.0 μM in HeLa, significantly lower than the 10.5 μM observed for their non-substituted analogue. In agreement with former studies, first generation dendrimers show similar or even higher potency despite bearing half of metal complexes, even though in this particular case the difference with generation 2 counterparts is not that clear. Both the methyl and the methoxy functions on the pyridine ring seem to improve the antitumor activity, especially when chloride is the counter-ion. It is also worth highlighting that, in general, the new Cu(II) iminopyridine metallodendrimers seem more efficient than the ruthenium(II) counterparts previously reported. For example, the first generation metallodendrimer bearing 4 Ru(II)-cymene complexes showed IC_{50} values 8.1±0.4 and 6.9±0.5 μM in HeLa and MCF-7, respectively [15], while the similar metallodendrimer with 4 Ru(II)-cyclopentadienyl complexes revealed IC_{50} values 6.3±0.2 and 10.3±0.5 μM, in HeLa and MCF-7 respectively [25]. The first generation Cu(II) metallodendrimers herein reported decrease those values to 1.9-2.6 μM in HeLa and 2.3-3.2 μM in MCF-7 cells.

2.3.2 In-depth evaluation of the biological effect of the metallodendrimers on U937 tumor cells and Peripheral Blood Mononuclear Cells (PBMCs)

On the basis of both the above described MTT tests, which confirmed the positive effect of the substituent on the cytotoxic activity, and the EPR results, which showed a stabilization of the $Cu\text{-}N_2O_2$ coordination for the first generation compounds, metallodendrimers $G_1(\text{-}CH_3)Cl$ **(8)**, $G_1(\text{-}OCH_3)Cl$ **(11)**, $G_1(\text{-}CH_3)NO_3$ **(14)** and $G_1(\text{-}OCH_3)NO_3$ **(17)** were subjected to more in-depth studies. Healthy PBMCs and U937 tumor cells were chosen for subsequent experiments to provide an accurate comparison with former studies [9]. In these experiments, cells were treated with the metallodendrimers at a concentration equivalent to the IC_{50} shown for MCF-7, to compare the effect of such concentration on a different kind of tumor cells and on healthy cells.

2.3.2.1 Cytotoxic and cytostatic effect through flow cytometry and confocal microscopy

Primarily, we investigated the cell death rate by means of ANX/7AAD test. Analyses were conducted by both flow cytometry (to quantitate the process in the whole biologic sample) and by confocal microscopy (to confirm and further characterize flow cytometric data). **Figures 4.A** and **4.B** depict the percentages of early apoptotic cells (AnxV positive), late apoptotic/necrotic cells (AnxV/7AAD positive) and ROS production in U937 and PBMC samples in absence (ct) and in presence of the dendrimers.

PBMCs showed a negligible increase of early apoptotic cells, compared to untreated cells, with a maximum percentage of 10% after treatment with $G_1(\text{-}CH_3)NO_3$ **(14).** U937 cells underwent an even smaller effect on early apoptotic cells but an outstanding increase on late apoptotic/necrotic cells after treatment with $G_1(\text{-}CH_3)Cl$ **(8)** (75%) and $G_1(\text{-}OCH_3)NO_3$ **(17)** (95%). For PBMCs, the highest percentage of late apoptotic/necrotic cells was

produced by $G_1(\text{-}OCH_3)Cl$ **(11)** (18%) and $G_1(\text{-}OCH_3)NO_3$ **(17)** (23%). These data clearly and significantly ($p<0,05$) demonstrated that metallodendrimers $G_1(\text{-}CH_3)Cl$ **(8)** and $G_1(\text{-}OCH_3)NO_3$ **(17)** strongly affected U937 viability, leaving the normal counterparts almost unaltered. Furthermore, as shown in **Fig. 4B** providing the Mitochondrial/Mitosox ROS for the various samples, PBMC were not only slightly affected by the dendrimers (max 23%), but also involved in an apparent non-necrotic process, as membrane blebbing (typical of apoptosis) confirmed (**Fig. 4.B** insert). Interestingly, these promising cytotoxic effects of metallodendrimers **8** and **17** correlate well with the higher stability of the $Cu\text{-}N_2O_2$ coordination and the good solubility (higher spectrum intensity) observed in EPR assays.

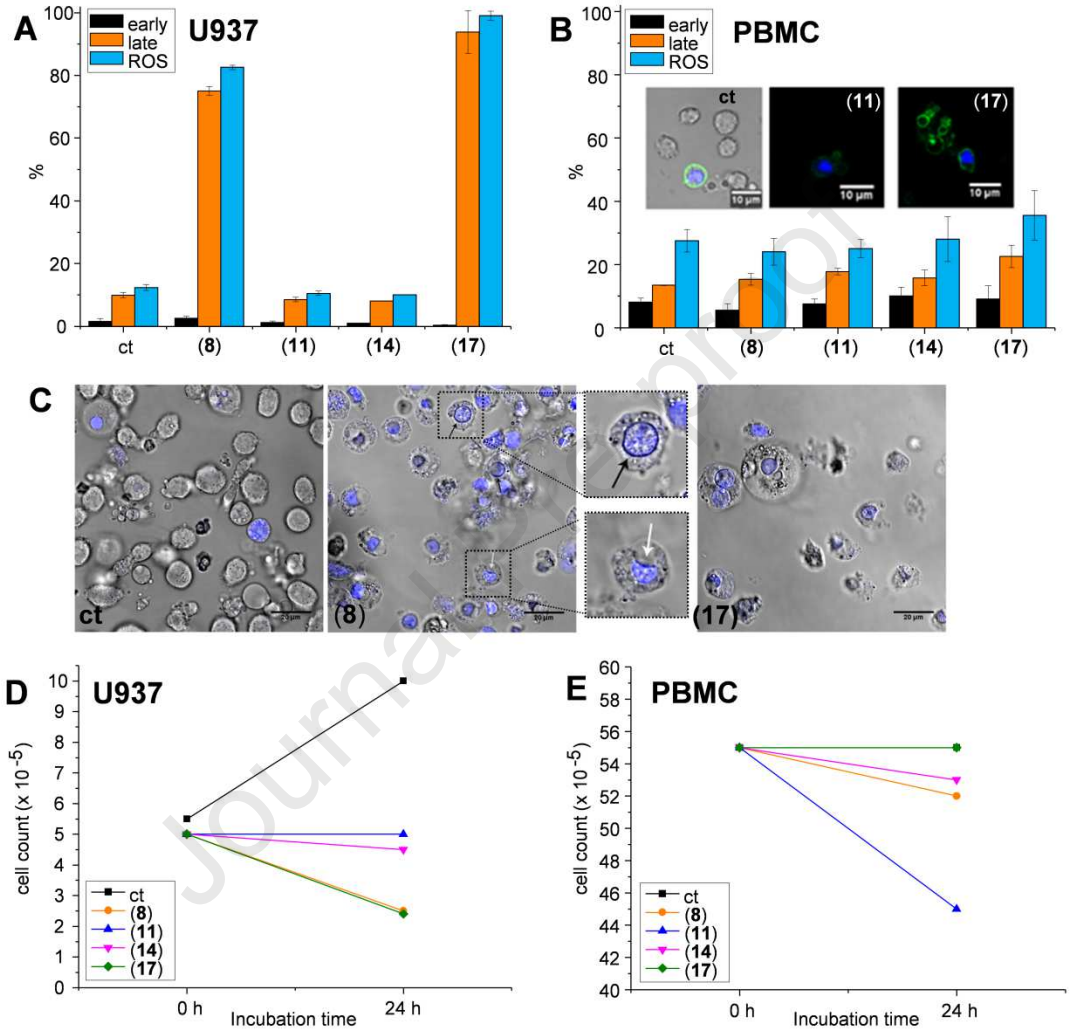

Figure 4. Cytotoxic and cytostatic effect of G1 metallodendrimers on tumor U937 cells and healthy PBMCs. (**A/B**) Percentage of early apoptotic cells (AnxV+, black columns); late apoptotic/necrotic cells (AnxV/7AAD+, orange columns) and ROS production (Mitochondrial/Mitosox ROS, blue columns). (**B**-insert) Single confocal optical sections of apoptotic cells in untreated and treated PBMCs. (**C**) Confocal images of untreated and treated U937 cells. Nuclei are stained by means of 7-AAD. Black arrow indicates chromatin margination and white arrow indicates cup shaped chromatin. (**D/E**) Change in absolute cell number, measuring the combined cytostatic/cytotoxic effect for U937 or the cytotoxic effect for PBMCs.

Metallodendrimer $G_1(\text{-}CH_3)Cl$ **(8)** induced a mixed phenomenon of necrosis and late apoptosis, as confocal images underlined (cup-shaped chromatin and chromatin margination besides the loss of membrane integrity and strong vacuolation, as shown in **Fig. 4.C**), whereas $G_1(\text{-}OCH_3)NO_3$ **(17)** effects were mainly necrotic. The evaluation of mitochondrial produced ROS by MitoSox (MS) labelling showed an overlapping trend with cell death data. In fact, in PBMCs we found a moderate degree of MS fluorescence for all molecules tested, starting from control cells expressing higher basal content of mitochondrial ROS. These values were negligible if compared with those from U937 cells treated with $G_1(\text{-}CH_3)Cl$ **(8)** and $G_1(\text{-}OCH_3)NO_3$ **(17)**. The scenario clearly involved ROS massive increase in cell death mechanisms exploited by U937 tumor cells.

The previous data were coupled with cell absolute counting to evaluate not only cytotoxic, but also cytostatic effects, particularly on U937 cells that are proliferating tumor cells (**Fig. 4.D/E**). It is possible to observe a drop in cell number with metallodendrimers $G_1(\text{-}CH_3)Cl$ **(8)**- and $G_1(\text{-}OCH_3)NO_3$ **(17)**- treated samples, which therefore showed a specific cytotoxic effect. Of note, also metallodendrimers in $G_1(\text{-}OCH_3)Cl$ **(11)** and $G_1(\text{-}CH_3)NO_3$ **(14)** induced an inhibition of proliferation.

In conclusion, a potent activity was observed for $G_1(\text{-}CH_3)Cl$ **(8)** and $G_1(\text{-}OCH_3)NO_3$ **(17)**, which significantly decreases for $G_1(\text{-}OCH_3)Cl$ **(11)** and $G_1(\text{-}CH_3)NO_3$ **(14)**. This crossed influence of the substituent/counterion might be explained considering the inductive and resonance properties produced by the substituents (**Figure 5**). For pyridine, the basicity of the nitrogen atom increases with the substituent in 4-position in the following trend: pyridine (pK_a 5.25) < 4-methylpyridine (pK_a 6.00) < 4-methoxopyridine (pK_a 6.47). The 4-methyl group produces a +I effect, while the 4-methoxo presents –I effect but with a predominant +M effect which delocalizes the negative charge in the nitrogen atom, increasing its basicity towards Lewis acids such as Cu(II). Cu(II) is a borderline acid with higher cationic character in the presence of nitrate counter-ions, compared to chloride ones. Accordingly, the strongest interaction will occur in $G_1(\text{-}OCH_3)NO_3$ **(17)** and can be therefore considered a "Cu(II)-donor". A clue to this behavior is confirmed by the CuO_4 component, arising mainly in nitrate complexes. This may explain the potent induction of apoptosis/necrosis and ROS production. In the presence of biological reductants, Cu(II) can be reduced to Cu(I) *via* Fenton-catalysed Haber-Weiss reaction, which may drive the generation of extremely toxic ·OH radicals, the most dangerous ROS in biological systems [26]. Other Cu(II)-complexes have been reported to induce apoptosis in cancer cells through the generation of ·OH radicals [27]. On the other hand, Cu(II) overloads produce respiratory inhibition and phospholipid peroxidation in mitochondria. Unbound copper ions may initiate redox cycling reactions, promote production of ROS such as superoxide, and create an oxidative environment capable of modifying the structure and function of biological macromolecules, thus threatening the functionality and viability of cells. In fact, in our model, a great excess of mitochondrial ROS (superoxide) was found, triggering a massive cell death on U937 cells, suggesting a double effect of copper, as both Cu(II) and Cu(I). Cu(II) can also react with thiol groups and glutathione, leading to $Cu(I)\text{-}(GSH)_2$ complexes, as reported by other groups [28].

On the other hand, the surprisingly high activity of $G_1(\text{-}CH_3)Cl$ **(8)** may be explained through a different mechanism. In this case, it is worth considering the increased lipophilicity (+π) produced by the methyl substituent [13]. The effect of the pyridine substituent on the permeability of Caco-2 monolayers has been previously studied and concluded that they are mainly dictated by aqueous desolvation [29]. The poorer dissociation of $CuCl_2$ also contributes to increase the overall lipophilicity of the metallodendrimer. Subsequently, the mechanism of action may be related to an increased interaction with tumor cell membranes, as observed in former studies with $G_n\text{-}[NCPh(o\text{-}N)CuCl_2{\cdot}H_2O]_m$ compared to their nitrate analogues [14]. Here, the high production of ROS may be triggered by the interaction with mitochondrial oxidative chain. Both these mechanisms lead to a great number of late apoptotic/necrotic cells and ROS, by taking two very different paths. Switching the ligands makes these mechanisms less effective, therefore lowering the antitumor activity.

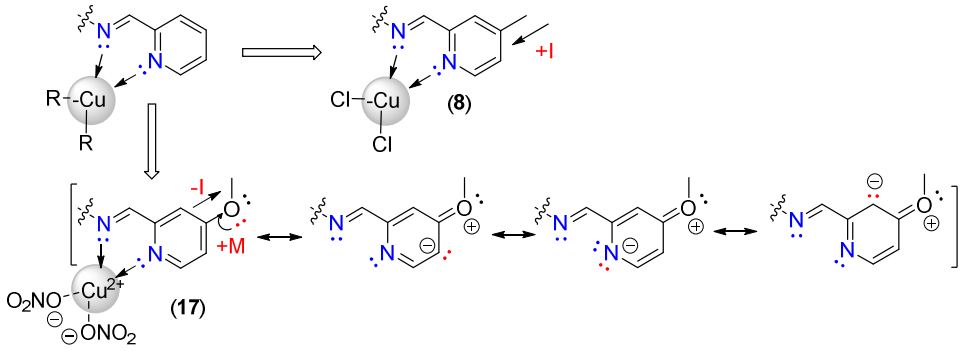

Figure 5. Proposed effects responsible of the increased cytotoxic activity of metallodendrimers **8** and **17**, compared to the non-substituted counterpart. Top: the increased overall lipophilicity in **8** due to +π and +I effects may improve the interaction with mitochondrial oxidative chain. Bottom: the stronger N-Cu interaction in **17** due to +M effect, may be efficient for Fenton reaction.

2.3.2.2 Impact on the mitochondria network, acidic vacuoles and surface molecule of U937 tumor cells

A more in-depth study was performed on U937 cells in order to find potential targets of the metallodendrimers. **Figure 6** depicts the mean fluorescence intensity (M.F.I.) of different probes in U937 cells after treatment with the metallodendrimers, measured through Flow Cytometry. Monodansylcadaverine (MDC) labels acidic endosomes, lysosomes, and late-stage autophagosomes. A significant decrease in the fluorescence of this probe was observed for U937 cells treated mainly with $G_1(\text{-}CH_3)Cl$ **(8)** and $G_1(\text{-}OCH_3)NO_3$ **(17)**, delineating a reduction in the number of these organelles. MitoTracker red (MTR) provides information about mitochondria-network. Again, the decrease in MTR fluorescence produced by **8** and **17** is related to the presence of an apoptotic process, in agreement with data on cytotoxic induction. Finally, possible effects on surface membrane molecules were tested using anti-CD11b antibody APC-conjugated (clone M1/70). CD11b is an integrin family member expressed on the surface of many leukocytes, including U937 myeloid tumor cells, considered a type of acute myeloid leukemia (AML) cell line [30]. The decrease of CD11b expression in such cells, mainly produced by **8** and **17**, revealed a shedding effect arising from the deep cell death induced by the dendrimers. However, cells treated with $G_1(\text{-}CH_3)NO_3$ **(14)** (revealing a main cytostatic effect), as $G_1(\text{-}OCH_3)Cl$ **(11)** showed a specifically-induced decrease in CD11b expression, that is observed on a single blood donor and it deserves to be deeply investigated on a larger population, in future experiments.

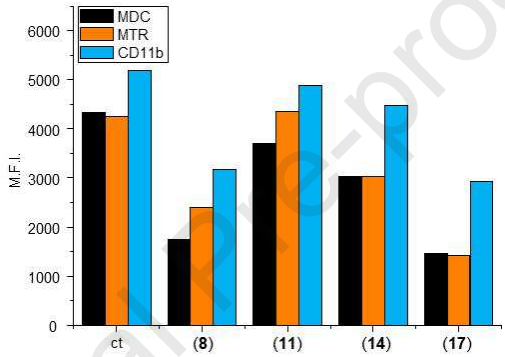

Figure 6. Effect of metallodendrimers treatment in U937 cells, measured as the change in the mean fluorescence intensity (M.F.I.) of monodansylcadaverine (MDC, black columns), measuring acidic vacuoles; MitoTracker red (MTR), detecting mitochondria network (MTR, orange columns); and CD11b, measuring its density on the surface membrane (blue columns).

2.3.2.3 Impact on PBMC subsets

To better evaluate the impact of these metallodendrimers on specific immunocompetent subsets, we labelled PBMCs using antiCD3 APC conjugated mAb (clone UCHT1), distinguishing CD3+ lymphocytes (T cytotoxic and T helper) from CD3- lymphocytes (Natural Killer +B). Although the metallodendrimers barely affected the viability of normal lymphocytes, these cells exhibited dissimilar basal values for both MTR and MDC fluorescence values and were differently modulated by the dendrimers (**Figure 7**). Firstly, the data pointed out that $G_1(\text{-}CH_3)Cl$ **(8)**, $G_1(\text{-}OCH_3)Cl$ **(11)** and $G_1(\text{-}OCH_3)NO_3$ **(17)** reduced CD3-fraction, revealing a slight increase in CD3+ lymphocytes, whereas the CD3-/CD3+ cells ratio bare the same of control cells for $G_1(\text{-}CH_3)NO_3$ **(14)**. Scarce are the data on literature regarding this aspect, suggesting a higher resistance for T lymphocytes. In particular, M.F.I. of MTR for CD3+ and CD3- lymphocytes in absence and presence of the dendrimers (**Fig. 6B**) shows that mitochondria network was more involved by the two molecules most affecting the tumor counterparts but in an opposite way: for $G_1(\text{-}CH_3)Cl$ **(8)** we observed a negative regulation of mitochondrial network, whereas there is an increase for $G_1(\text{-}OCH_3)NO_3$ **(17)**. $G_1(\text{-}CH_3)NO_3$ **(14)** did not affect CD3+ lymphocytes but targeted mitochondria in CD3- PBMCs. Although MitoTracker Dyes label mitochondria structure and morphology, they are not insensitive to mitochondrial membrane potential. In particular, **Fig. 7B** shows a relevant decrease of MTR MFI for **8**-treated cells in both CD3- and CD3+ subpopulations.

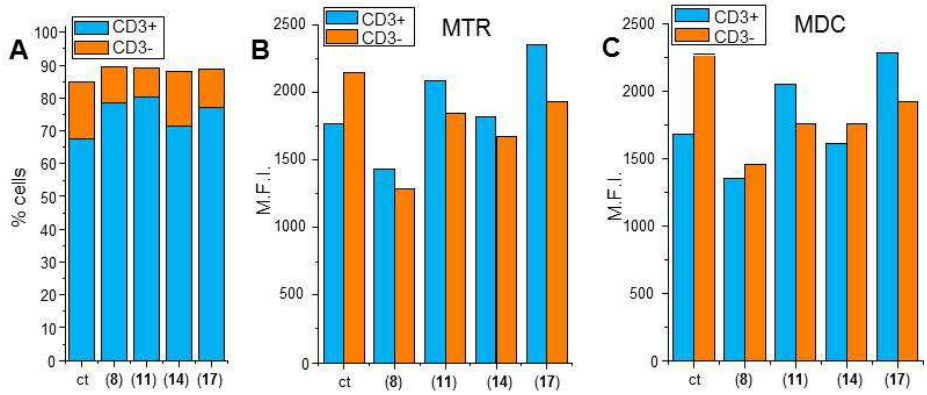

Figure 7. Effect of metallodendrimers treatment in PBMC subpopulations. (A) Percentage of CD3+ and CD3- lymphocytes; (B/C) change in the mean fluorescence intensity (M.F.I.) of MitoTracker red (MTR), detecting mitochondria network, and monodansylcadaverine, measuring acidic vacuoles.

With respect to the autophagic acidic vacuoles (AVs, **Fig. 7C**), we firstly detected the basal condition (ct, non-treated cells) in which they are more abundant in CD3-lymphocytes. These data are in agreement with previous literature [31]. Autophagy has recently emerged as crucial for the maintenance of certain B cell populations (i.e., memory B cells and plasma cells), while its role in the development and survival of naïve B cells remains largely to be elucidated. Conversely, the role of autophagy at late stages of B cell differentiation is well established [32, 33]. Also, for Natural Killer (NK) cell, it is possible to highlight a key role for autophagy in the regulation of the innate immune system [34], shared with neutrophils, eosinophils and mast cells.

Figure 7.C reveals that AV content in CD3- fraction was downregulated by all dendrimers investigated, whereas **11** and **17** induced an upregulation in CD3+ lymphocytes. These two compounds, **11** and **17**, also positively modulated MTR fluorescence. Several studies have shown that autophagy is increased in T cells upon activation [35] and autophagy has been shown to adjust its cargo selection upon T-cell activation. Although intriguing, these data are from series of test of the same blood donor: this implies that, in this case, we do not take into account the biological variability. However, the impact of our results is relevant, since this analytical strategy may improve data on such anticancer molecules and indeed, since the immunologic aspect is mandatory in fighting against cancer.

3. Conclusions

The search for a rationale in the therapy against cancer requires the study of molecules with a precise structure-to-property relationship, in order to highlight sound interactions with both healthy and tumor cells. Cu(II)-conjugated metallodendrimers are promising candidates, featuring high stability and extraordinary versatility. Furthermore, they are an extraordinary tool to analyze structure-to-property relationships, such as dendrimer generation, metal counterions and iminopyridine substituents, as herein described. EPR studies provided valuable information about the behavior of the metallodendrimers in solution: they depict different coordination modes of the Cu(II) ion (Cu-N_2O_2, Cu-N_4 and Cu-O_4), whose relative percentages are determined by the structural features of the dendritic molecules. Through our studies we concluded that the most promising metallodendrimers - G_1(-CH_3)Cl **(8)** and G_1(-OCH_3)NO_3 **(17)**, minimized the Cu-N_4 coordination in favour of Cu-N_2O_2 complexes. Furthermore, we found a surprising crossed-influence of substituent/counterion on the antitumor activity of Cu(II)-metallodendrimers, which increased the activity compared to the non-substituted counterparts. This set the foundations for potentially two different mechanisms of action for the production of ROS in myeloid tumor cells, while barely affecting healthy cells. This potential selectivity towards cancer cells has been described for other copper complexes [7] and highlights the potential use of these metallodrugs as alternative to cisplatin. Nevertheless, this fact is even more remarkable in non-solid tumors like the myeloid cancer here evaluated, which cannot benefit from the Enhanced Permeation and Retention Effect produced by nanoparticles. Importantly, preliminary studies revealed that our Cu(II) metallodendrimers may modulate the different subsets of immunocompetent PBMCs. The effect on these subsets, comprising cells able to produce antibodies (B cells [36]) and cells able to induce cytotoxicity (CD8+ and NK cells [37]), requires a more in-depth evaluation to understand the full potential of these new metallodrugs.

4. Materials and Methods

2.1 Synthesis and Characterization

Solvents were purified from appropriate drying agents. Chemicals were purchased from commercial sources and used as received. Elemental analyses were performed on a LECO CHNS-932. Fourier transform-infrared (FT-IR) spectra were registered with a Cary 630 FTIR Agilent spectrophotometer equipped with an attenuated total reflectance (ATR) sampling accessory with a diamond crystal. The instrument was controlled with Agilent Microlab PC software and spectra were recorded in the 4000–400 cm^{-1} range. Mass Spectra were obtained from an Agilent 6210 spectrometer. EPR spectra were recorded by means of an EMX-Bruker spectrometer operating at X band (9.5 GHz) and interfaced with a PC (software from Bruker for handling the EPR spectra). The temperature was controlled with a Bruker ST3000 variable-temperature assembly cooled with liquid nitrogen.

2.1.1 Synthesis and characterization of dendrimers featuring substituted iminopyridine ligands

G_0-[NCPh(*m*-CH_3)(*o*-N)] (1). A dry THF solution of compound 2-Formyl-4-picoline (59.3 mg, 0.489 mmol) was added to a dry THF solution of G_0-[NH_2] **(I)** (84.8 mg, 0.489 mmol), in the presence of $MgSO_4$ to trap water produced during the reaction. After 12 h reaction at r.t. stirring under inert atmosphere, the orange solution was filtrated to remove the $MgSO_4$. Solvent was then evaporated to dryness and compound **1** was isolated as yellowish oil (106.9 mg, 79%). ^{1}H-NMR ($CDCl_3$): δ (ppm) 0.52 (m, 9H, -Si($CH_2C\mathbf{H}_3)_3$); 0.92 (overlapping m, 8H, -Si($C\mathbf{H}_2CH_3)_3$ and -Si$C\mathbf{H}_2CH_2$); 1.71 (m, 2H, - Si$CH_2C\mathbf{H}_2CH_2N$); 2.38 (s, 3H, Ar-$C\mathbf{H}_3$); 3.64 (t, 2H, -$CH_2C\mathbf{H}_2N$); 7.12 (dd, J = 3, 5.0 Hz, J = 4, 0.9 Hz, 1H, Ar); 7.81 (s, 1H,Ar); 8.48 (d, 1H, Ar); 8.35 (s, 1H, -$C\mathbf{H}_{imine}$). ^{13}C-{^{1}H} NMR ($CDCl_3$): δ (ppm) 3.24 (-Si($CH_2\mathbf{C}H_3)_3$); 7.42 (-Si($\mathbf{C}H_2CH_3)_3$); 8.98 (-Si$\mathbf{C}H_2CH_2$); 20.95 (Ar-**C**H3); 25.30 (-$CH_2\mathbf{C}H_2CH_2$); 65.17 (-$CH_2\mathbf{C}H_2N$); 121.75, 125.62, 147.76, 149.15, 161.96 (**C**Ar); 154.43 (-$\mathbf{C}H_{imine}$). Elemental analysis ($C_{16}H_{28}N_2Si$); calc. (%): C, 69.50; H, 10.21; N, 10.13. Exp. (%): C, 68.29; H, 9.86; N, 9.64. IR spectroscopy, v(C=N): 1600.6 cm^{-1}.

G_1-[NCPh(*m*-CH_3)(*o*-N)]$_4$ (2). First generation dendrimer **2** was synthesized following the same protocol described above, using the reagents: G_1-[NH_2]$_4$ **(II)** (222.0 mg, 0.336 mmol) and 2-Formyl-4-picoline (162.8 mg, 1.344 mmol). Compound **2** was isolated as yellowish oil (230.9 mg, 64%). ^{1}H-NMR ($CDCl_3$): δ (ppm) 0.05 (s, 24H, -($C\mathbf{H}_3)_2SiCH_2CH_2CH_2N$); 0.52 (overlapping m, 24H, -Si$C\mathbf{H}_2CH_2C\mathbf{H}_2$Si and - Si$C\mathbf{H}_2CH_2CH_2N$); 1.28 (m, 8H, -Si$CH_2C\mathbf{H}_2CH_2$Si); 1.68 (m, 8H, -Si$CH_2C\mathbf{H}_2CH_2N$); 2.36 (s, 3H, Ar-$C\mathbf{H}_3$); 3.62 (m, 8H, -($CH_3)_2SiCH_2CH_2C\mathbf{H}_2N$); 7.09 (m, 4H, Ar); 7.79 (m, 4H, Ar); 8.46 (m, 4H,Ar); 8.32 (s, 4H, -$C\mathbf{H}_{imine}$). ^{13}C-{^{1}H} NMR ($CDCl_3$): δ (ppm) 1.22 (-($\mathbf{C}H_3)_2SiCH_2CH_2CH_2N$); 13.30 (-Si$\mathbf{C}H_2CH_2CH_2N$); 17.75, 18.76, 20.38 (-Si$\mathbf{C}H_2C\mathbf{C}H_2$Si); 21.17 (Ar-**C**H3); 25.56 (-Si$CH_2\mathbf{C}H_2CH_2N$); 65.22 (-Si$CH_2CH_2\mathbf{C}H_2N$); 121.98, 125.82, 147.94, 149.37, 162.14 (**C**Ar); 154.65 (-$\mathbf{C}H_{imine}$). Elemental analysis ($C_{60}H_{100}N_8Si_5$). Calc. (%): C, 67.10; H, 9.39; N, 10.43. Exp. (%): C, 65.69; H, 8.92; N, 8.54. IR spectroscopy, v(C=N): 1605.9 cm^{-1}.

G_2-[NCPh(*m*-CH_3)(*o*-N)]$_8$ (3). Second generation dendrimer **3** was synthesized following to the same protocol described above, using the reagents: G_2-[NH_2]$_8$ **(III)** (265.1 mg, 0.161 mmol) and 2-Formyl-4-picoline (155.8 mg, 1.286 mmol). Compound **3** was isolated as yellowish oil (178.0 mg, 45%). ^{1}H-NMR ($CDCl_3$): δ (ppm) -0.12 (s, 12H, -$C\mathbf{H}_3SiCH_2CH_2CH_2$Si); -0.07 (s, 48H, -($C\mathbf{H}_3)_2SiCH_2CH_2CH_2N$); 0.51 (overlapping br m, 64H, -Si$C\mathbf{H}_2CH_2C\mathbf{H}_2$Si, -$CH_3SiC\mathbf{H}_2CH_2C\mathbf{H}_2$Si and -($CH_3)_2SiC\mathbf{H}_2CH_2CH_2N$); 1.28 (overlapping br m, 24H, -Si$CH_2C\mathbf{H}_2CH_2$Si and - $CH_3SiCH_2C\mathbf{H}_2CH_2$Si); 1.67 (br m, 16H, -($CH_3)_2SiCH_2C\mathbf{H}_2CH_2N$); 2.34 (s, 3H, Ar-$C\mathbf{H}_3$); 3.60 (m, 16H, -($CH_3)_2SiCH_2CH_2C\mathbf{H}_2N$); 7.08 (m, 8H, Ar); 7.78 (m, 8H, Ar); 8.44 (m, 8H, Ar); 8.31 (s, 8H, -$C\mathbf{H}_{imine}$). ^{13}C-{^{1}H}-NMR ($CDCl_3$): δ(ppm) -4.95 (-($\mathbf{C}H_3)_2SiCH_2CH_2CH_2N$); -3.29 (-$\mathbf{C}H_3SiCH_2CH_2CH_2$Si); 13.07 (-($CH_3)_2Si\mathbf{C}H_2CH_2CH_2N$); 17.70, 18.44, 18.59, 18.81, 19.20, 20.02 (-Si$\mathbf{C}H_2C\mathbf{C}H_2C\mathbf{C}H_2Si_{core}$ and -$CH_3Si\mathbf{C}H_2C\mathbf{C}H_2C\mathbf{C}H_2$Si); 20.96 (-($CH_3)_2SiCH_2\mathbf{C}H_2CH_2N$); 25.33 (Ar-**C**H3); 64.98 (-($CH_3)_2SiCH_2CH_2\mathbf{C}H_2N$); 121.75, 125.59, 147.68, 149.14, 161.91 (C_{Ar}); 154.42 (-$\mathbf{C}H_{imine}$). Elemental analysis ($C_{136}H_{236}N_{16}Si_{13}$). Calc. (%): C, 66.39; H, 9.67; N, 9.11. Exp. (%): C, 66.05; H, 9.59; N, 9.27. IR spectroscopy, v(C=N): 1605.9 cm^{-1}.

G_0-[NCPh(*m*-OCH_3)(*o*-N)] (4). Compound **4** was synthesized following the same protocol described above, using the reagents: G_0-[NH_2] **(I)** (347.1 mg, 2.003 mmol) and 4-Methoxy-2-pyridinecarbaldehyde (274.6 mg, 2.003 mmol). Compound **4** was isolated as yellowish oil (474.6 mg, 81%). ^{1}H-NMR ($CDCl_3$): δ (ppm) 0.52 (m, 9H, -Si($CH_2C\mathbf{H}_3)_3$); 0.92 (overlapping m, 8H, -Si($C\mathbf{H}_2CH_3)_3$ and -Si$C\mathbf{H}_2CH_2$); 1.71 (m, 2H, - Si$CH_2C\mathbf{H}_2CH_2N$); 3.64 (m, 2H, -$CH_2C\mathbf{H}_2N$); 3.89 (s, 3H, Ar-O-$C\mathbf{H}_3$); 6.83 (dd, J = 3, 5.7 Hz, J = 4, 2.6 Hz, 1H, Ar); 7.51 (m, 1H,Ar); 8.43 (d, 1H, Ar); 8.33 (s, 1H, -$C\mathbf{H}_{imine}$). ^{13}C-{^{1}H} NMR ($CDCl_3$): δ (ppm) 3.20 (-Si($CH_2\mathbf{C}H_3)_3$); 7.38 (-Si($\mathbf{C}H_2CH_3)_3$); 8.88

(-Si**C**H_2CH_2); 25.22 (-CH_2**C**H_2CH_2); 55.28 (Ar-O-**C**H3); 64.96 (-CH_2**C**H_2N); 105.42, 112.05, 150.31, 161.73, 166.13 (**C**Ar); 156.53 (-**C**H_{imine}). Elemental analysis ($C_{16}H_{28}N_2OSi$). Calc. (%): C, 65.70; H, 9.65; N, 9.58. Exp. (%): C, 64.20; H, 8.961; N, 8.676. ESI-TOF: m/z calc. 292.197 u; exp. 293.2029 u. IR spectroscopy, ν(C=N): 1602.6 cm^{-1}.

G_1-[NCPh(*m*-OCH_3)(*o*-N)]$_4$ (5). First generation dendrimer **5** was synthesized following the same protocol described above, using the reagents: G_1-[NH_2]$_4$ **(II)** (205.5 mg, 0.311 mmol) and 4-Methoxy-2-pyridinecarbaldehyde (170.4 mg, 1.242 mmol). Compound **5** was isolated as yellowish oil (219.2 mg, 62%).^{1}H-NMR ($CDCl_3$): δ (ppm) 0.04 (s, 24H, -(C**H**$_3$)$_2$SiCH$_2$CH$_2$CH$_2$N); 0.52 (overlapping m, 24H, -SiC**H**$_2$CH$_2$C**H**$_2$Si and - SiC**H**$_2$CH$_2$CH$_2$N); 1.27 (m, 8H, -SiCH$_2$C**H**$_2$CH$_2$Si); 1.67 (m, 8H, -SiCH$_2$C**H**$_2$CH$_2$N); 3.61 (m, 8H, -(CH$_3$)$_2$SiCH$_2$CH$_2$C**H**$_2$N); 3.85 (s, 3H, Ar-O-C**H**$_3$); 6.80 (m, 4H, Ar); 7.47 (m, 4H, Ar); 8.39 (m, 4H, Ar); 8.29 (s, 4H, -C**H**$_{imine}$). ^{13}C-{^{1}H} NMR ($CDCl_3$): δ (ppm) -3.35 (-(**C**H$_3$)$_2$SiCH$_2$CH$_2$CH$_2$N); 13.07 (-Si**C**H$_2$CH$_2$CH$_2$N); 17.52, 18.53, 20.15 (-Si**C**H$_2$**C**H$_2$**C**H$_2$Si); 25.30 (-SiCH$_2$**C**H$_2$CH$_2$N); 55.31 (s, 3H, Ar-O-**C**H$_3$); 64.86 (-SiCH$_2$CH$_2$**C**H$_2$N); 105.56, 112.01, 150.34, 161.73, 166.15, (**C**Ar); 156.51 (- **C**H$_{imine}$). Elemental analysis ($C_{60}H_{100}N_8O_4Si_5$). Calc. (%): C, 63.33; H, 8.86; N, 9.85. Exp. (%): C, 61.67; H, 8.87; N, 8.84. IR spectroscopy, ν(C=N): 1587.2 cm^{-1}.

G_2-[NCPh(*m*-OCH_3)(*o*-N)]$_8$ (6). Second generation dendrimer **6** was synthesized following to the same protocol described above, using the reagents: G_2-[NH_2]$_8$ **(III)** (265.1 mg, 0.107 mmol) and 4-Methoxy-2-pyridinecarbaldehyde (117.1 mg, 0.854 mmol). Compound **5** was isolated as yellowish oil (118.9 mg, 43%).^{1}H-NMR ($CDCl_3$): δ (ppm) -0.11 (s, 12H, -C**H**$_3$SiCH$_2$CH$_2$CH$_2$Si); -0.06 (s, 48H, -(C**H**$_3$)$_2$SiCH$_2$CH$_2$CH$_2$N); 0.51 (overlapping br m, 64H, -SiC**H**$_2$CH$_2$C**H**$_2$Si, -CH$_3$SiC**H**$_2$CH$_2$C**H**$_2$Si and - (CH$_3$)$_2$SiC**H**$_2$CH$_2$CH$_2$N); 1.28 (overlapping br m, 24H, -SiCH$_2$C**H**$_2$CH$_2$Si and - CH$_3$SiCH$_2$C**H**$_2$CH$_2$Si); 1.67 (br m, 16H, -(CH$_3$)$_2$SiCH$_2$C**H**$_2$CH$_2$N); 3.61 (m, 16H, -(CH$_3$)$_2$SiCH$_2$CH$_2$C**H**$_2$N); 3.86 (s, 3H, Ar-O-C**H**$_3$); 6.81 (m, 8H, Ar); 7.48 (m, 8H, Ar); 8.40 (m, 8H, Ar); 8.29 (s, 8H, -C**H**$_{imine}$). ^{13}C-{^{1}H}-NMR ($CDCl_3$): δ(ppm) -4.75 (-(**C**H$_3$)$_2$SiCH$_2$CH$_2$CH$_2$N); -3.09 (-**C**H$_3$SiCH$_2$CH$_2$CH$_2$Si); 13.28 (-(CH$_3$)$_2$Si**C**H$_2$CH$_2$CH$_2$N); 18.66, 19.02, 20.24, (-Si**C**H$_2$**C**H$_2$**C**H$_2$Si$_{core}$ and -CH$_3$Si**C**H$_2$**C**H$_2$**C**H$_2$Si); 25.52 (-(CH$_3$)$_2$SiCH$_2$**C**H$_2$CH$_2$N); 55.52 (Ar-O-**C**H$_3$); 65.09 (-(CH$_3$)$_2$SiCH$_2$CH$_2$**C**H$_2$N); 105.78, 112.22, 156.74, 161.95, 166.36 (C_{Ar}); 150.57 (-**C**H$_{imine}$). Elemental analysis ($C_{136}H_{236}N_{16}O_8Si_{13}$). Calc. (%):C, 62,73; H, 9.10; N, 8.80. Exp. (%): C, 60.11; H, 8.37; N, 7.44. IR spectroscopy, ν(C=N): 1594.5 cm^{-1}.

2.1.2 Synthesis and structural characterization of Cu(II) metallodendrimers

G_0-[NCPh(*m*-CH_3)(*o*-N)$CuCl_2$·$2H_2O$] (7). A methanol solution of compound G_0-[NCPh(*m*-CH_3)(*o*-N)] (**1**) (50.9 mg, 0.184 mmol) was dropwise added to a methanol solution of $CuCl_2$·$2H_2O$ (31.4 mg, 0.184 mmol). After 1.5 h of reaction under stirring at r.t., solvent was evaporated to dryness and compound **7** was isolated as green solid (67.5 mg, 85%). Elemental analysis ($C_{16}H_{30}Cl_2CuN_2OSi$). Calc. (%): C, 44.80; H, 7.05; N, 6.53. Exp. (%): C, 44.31; H, 6.54; N, 6.23. IR spectroscopy, ν(C=N): 1623.0 cm^{-1}.

G_1-[NCPh(*m*-CH_3)(*o*-N)$CuCl_2$·H_2O]$_4$ (8). First generation metallodendrimer **8** was synthesized following to the same protocol described above, using the reagents: G_1-[NCPh(*m*-CH_3)(*o*-N)] (**2**) (123.3 mg, 0.115 mmol) and $CuCl_2$·$2H_2O$ (78.4 mg, 0.459 mmol). Compound **8** was isolated as green solid (127.2 mg, 66%). Elemental analysis ($C_{60}H_{108}Cl_8Cu_4N_8O_4Si_5$). Calc. (%): C, 42.80; H, 6.47; N, 6.66. Exp. (%): C, 43.26; H, 6.07; N, 6.85. IR spectroscopy, ν(C=N): 1612.8 cm^{-1}.

G_2-[NCPh(*m*-CH_3)(*o*-N)$CuCl_2$·H_2O]$_8$ (9). Second generation metallodendrimer **9** was synthesized following the same protocol described above, using the reagents: G_2-[NCPh(*m*-CH_3)(*o*-N)] (**3**) (170.8 mg, 0.069 mmol) and $CuCl_2$·$2H_2O$ (94.7 mg, 0.519 mmol). Compound **9** was isolated as green solid (147.3 mg, 58%). Elemental analysis ($C_{136}H_{252}Cl_{16}Cu_8N_{16}O_8Si_{13}$). Calc. (%): C, 44.38; H, 6.90; N, 6.09. Exp. (%): C, 42.22; H, 6.52; N, 5.77. IR spectroscopy, ν(C=N): 1613.9 cm^{-1}.

G_0-[NCPh(*m*-OCH_3)(*o*-N)$CuCl_2$·H_2O] (10). Compound **10** was synthesized following the protocol described above, using the reagents: G_0-[NCPh(*m*-CH_3)(*o*-N)] (**1**) (81.4 mg, 0.278 mmol) and Cu(NO$_3$)$_2$·$3H_2O$ (47.4 mg, 0.278 mmol). Compound **10** was isolated as blue solid (107.4 mg, 87%). Elemental analysis ($C_{16}H_{30}CuN_4O_7Si$). Calc. (%): C, 43.19; H, 6.80; N, 6.30. Exp. (%): C, 44.49; H, 6.18; N, 6.61. IR spectroscopy, ν(C=N): 1609.5 cm^{-1}.

G_1-[NCPh(*m*-OCH_3)(*o*-N)$CuCl_2$·H_2O]$_4$ (11) First generation metallodendrimer **11** was synthesized following to the same protocol described above, using the reagents: G_1-[NCPh(m-CH_3)(o-N)] (**2**) (145.0 mg, 0.127 mmol) and Cu(ONO_2)$_2$·$3H_2O$ (86.9 mg, 0.510 mmol). Compound **11** was isolated as blue solid (129.9 mg, 58%). Elemental analysis ($C_{60}H_{108}Cu_4N_{16}O_{28}Si_5$). Calc. (%): C, 41.23; H, 6.23; N, 6.41. Exp. (%): C, 40.85; H, 5.88; N, 6.25. IR spectroscopy, ν(C=N): 1618.8 cm^{-1}.

G_2-[NCPh(*m*-OCH_3)(*o*-N)$CuCl_2{\cdot}H_2O]_8$ (12). Second generation metallodendrimer **12** was synthesized following the same protocol described above, using the reagents: G_2-[NCPh(*m*-CH_3)(*o*-N)] (**3**) (248.1 mg, 0.097 mmol) and $Cu(NO_3)_2{\cdot}3H_2O$ (130.7 mg, 0.776 mmol). Compound **12** was isolated as blue solid (260.0 mg, 70%). Elemental analysis ($C_{136}H_{252}Cu_8N_{32}O_{56}Si_{13}$). Calc. (%): C, 42.89; H, 6.67; N, 5.88. Exp. (%): C, 40.19; H, 6.10; N, 5.49. IR spectroscopy, v(C=N): 1615.6 cm^{-1}.

G_0-[NCPh(*m*-CH_3)(*o*-N)$Cu(ONO_2)_2{\cdot}H_2O$] (13). Metal complex **13** was synthesized following the protocol described above, using the reagents: G_0-[NCPh(*m*-OCH_3)(*o*-N)] (**4**) (40.8 mg, 0.147 mmol) and $CuCl_2{\cdot}2H_2O$ (35.6 mg, 0.147 mmol). Compound **13** was isolated as green solid (65.0 mg, 91%). Elemental analysis ($C_{16}H_{30}Cl_2CuN_2O_2Si$). Calc. (%): C, 38.58; H, 6.07; N, 11.25. Exp. (%): 35.98; H, 5.40; N, 11.03. IR spectroscopy, v(C=N): 1615.8 cm^{-1}.

G_1-[NCPh(*m*-CH_3)(*o*-N)$Cu(ONO_2)_2{\cdot}H_2O]_4$ (14). First generation metallodendrimer **14** was synthesized following the same protocol described above, using the reagents: G_1-[NCPh(*m*-OCH_3)(*o*-N)] (**5**) (90.7 mg, 0.084 mmol) and $CuCl_2{\cdot}2H_2O$ (81.6 mg, 0.338 mmol). Compound **14** was isolated as green solid (104.6 mg, 65%). Elemental analysis ($C_{60}H_{108}Cl_8Cu_4N_8O_8Si_5$). Calc. (%): C, 38.01; H, 5.74; N, 11.82. Exp. (%): C, 37.37; H, 5.37; N, 11.60. IR spectroscopy, v(C=N): 1618.9 cm^{-1}.

G_2-[NCPh(*m*-CH_3)(*o*-N)$Cu(ONO_2)_2{\cdot}H_2O]_8$ (15). Second generation metallodendrimer **15** was synthesized following the same protocol described above, using the reagents: G_2-[NCPh(*m*-OCH_3)(*o*-N)] (**6**) (175.9 mg, 0.071 mmol) and $CuCl_2{\cdot}2H_2O$ (138.2 mg, 0.572 mmol). Compound **12** was isolated as green solid (135.5 mg, 75%). Elemental analysis ($C_{136}H_{252}Cl_{16}Cu_8N_{16}O_{16}Si_{13}$). Calc. (%): C, 39.79; H, 6.19; N, 10.92. Exp. (%): C, 38.1; H, 6.16; N, 10.53. IR spectroscopy, v(C=N): 1615.6 cm^{-1}.

G_0-[NCPh(*m*-OCH_3)(*o*-N)$Cu(ONO_2)_2{\cdot}H_2O$] (16). Metal complex **16** was synthesized following to the same protocol described above, using the reagents: G_0-[NCPh(*m*-OCH_3)(*o*-N)] (**4**) (74.5 mg, 0.255 mmol) and $Cu(NO_3)_2{\cdot}3H_2O$ (61.5 mg, 0.255 mmol). Compound **16** was isolated as blue solid (117.5 mg, 93%). Elemental analysis ($C_{16}H_{30}CuN_4O_8Si$). Calc. (%): C, 39.86; H, 6.27; N, 11.62. Exp. (%): C, 38.86; H, 5.80; N, 11.18. IR spectroscopy, v(C=N): 1609.5 cm^{-1}.

G_1-[NCPh(*m*-OCH_3)(*o*-N)$Cu(ONO_2)_2{\cdot}H_2O]_4$ (17). First generation metallodendrimer **17** was synthesized following the same protocol described above, using the reagents: G_1-[NCPh(*m*-OCH_3)(*o*-N)] (**5**) (134.5 mg, 0.118 mol) and $Cu(NO_3)_2{\cdot}3H_2O$ (114.4 mg, 0.473 mmol). Compound **17** was isolated as blue solid (138.0 mg, 60%). Elemental analysis ($C_{60}H_{108}Cu_4N_{16}O_{32}Si_5$). Calc. (%): C, 36.76; H, 5.55; N, 11.43. Exp. (%): C, 32.10; H, 4.925; N, 11.15. IR spectroscopy, v(C=N): 1608.3 cm^{-1}.

G_2-[NCPh(*m*-OCH_3)(*o*-N)$Cu(ONO_2)_2{\cdot}H_2O]_8$ (18). Second generation metallodendrimer **18** was synthesized following the same protocol described above, using the reagents: G_2-[NCPh(*m*-CH_3)(*o*-N)] (**6**) (261.9 mg, 0.101 mmol) and $Cu(NO_3)_2{\cdot}3H_2O$ (195.5 mg, 0.809 mmol). Compound **18** was isolated as blue solid (344.9 mg, 80%). Elemental analysis ($C_{136}H_{252}Cu_8N_{32}O_{64}Si_{13}$). Calc. (%): C, 38.59; H, 6.0; N, 10.59. Exp. (%): C, 37.99; H, 5.73; N, 10.72. IR, v(C=N): 1611.5 cm^{-1}.

2.2 EPR Analysis

2.2.1 Sample preparation

Dendrimers were used at a concentration of 0.5 mM in surface groups. Each sample was prepared by dissolving the weighted amount of dendrimer in DMSO and then diluting with distilled water to finally get a 3% DMSO-water solution. The sample was stirred for 15 minutes and then analyzed.

2.2.2 EPR Instrumentation

EPR spectra were recorded by means of an EMX-Bruker spectrometer operating at X band (9.5 GHz) and interfaced with a PC software WinEPR for spectra acquisition and handing, from Bruker (Bruker BioSpin, Rheinstetten, Germany). The temperature was controlled with a Bruker ST3000 variable-temperature assembly cooled with liquid nitrogen. The spectra were recorded at 37 °C ± 1. The spectra were considered valid if reproducible in at least three repeated experiments on the same sample.

2.2.3 Computation and Analysis of EPR Spectra

The following parameters were obtained via the computational procedure proposed by Budil *et al*. [18]: (a) The A_{ii} components of the **A** tensor for the coupling between the electron spin and the nuclear spin of the Cu(II). (b) The gii components of the **g** tensor for the coupling between the electron spin and the Cu(II) nuclear spin. (c) The correlation time for the rotational motion, τ, measured the microviscosity of the Cu(II) environment. The error was ± 0.01 ns, and was calculated by computation, that is, as indicated in (a), with values exceeding the error producing a worse fit between the experimental and the computed spectra. (d) Finally, the total intensity of well reproducible EPR spectra was evaluated by the double integral of the spectra and scaled to 100, assuming intensity = 100 for the spectrum at the highest intensity. Quantitative EPR measurements of spin concentration cannot be performed in the absence of an internal reference, but, in the present case, we trusted the intensity values only in a comparative way for a series of sample

2.3 Biological Assays

2.3.1. Cell Lines and Primary Cultures

Tumor cell lines from cervix (HeLa) and breast cancer (MCF-7) were seeded in 96-well plates (Nunclon Delta Surface, Thermo Fischer Scientific; 1.5 × 10^5 cells/ml) and grown for 24 h in 90 µl of complete medium (DMEM, sigma ref. D1408) supplemented with 10% Fetal Bovine Serum (sigma ref. F7524) and antibiotic/antimicotic solution (Pen/Stept/Ampho, Sigma ref. A5955).

Human PBMCs (peripheral blood mononuclear cells) were isolated from buffy coats of anonymized donors obtained from the Transfusion Center of Urbino Hospital. No specific approval from an institutional review board was required considering that: (1) no personal patient information was made available; (2) buffy coats could not be used for the treatment of patients and were waste products for the blood transfusion center; (3) blood donors were verbally informed that parts of the donation that cannot be used for patient treatment may be used for scientific research. PBMCs were isolated from buffy coats through density gradient separation using Lymphoprep solution (specific density, 1.077; Axis-Shield PoC AS, Oslo, Norway). Cells were washed twice in phosphate buffer saline (PBS) by centrifugation at 400g and suspended in RPMI-1640 with 10% (v/v) heat-inactivated fetal bovine serum (FBS), 100 µg/mL penicillin, 100 µg/Ml streptomycin, and 2 mM L-glutamine.

The U937 cell line (Sigma-Aldrich, USA) was grown in the RPMI-1640 medium supplemented with 10% (v/v) heat inactivated FBS, 100 U/mL penicillin, 100 µg/mL streptomycin, and 2 mM L-glutamine, at 37 °C in humidified air with 5% CO_2.

For PBMC and U937 experiments, solutions of compounds were prepared by diluting a stock solution of DMSO-Water (2% v/v), with the same volume of cell culture. The final DMSO concentration is therefore 1% v/v.

2.3.2. In vitro cell viability through colorimetric experiments

MTT assay. Tumor cell lines HeLa and MCF-7 were seeded in 96-well plates (Nunclon Delta Surface, Thermo Fischer Scientific; 1.5 × 10^5 cells/ml) and grown for 24 h in 90 µl of complete DMEM. Solutions of compounds were prepared by diluting a freshly prepared stock solution in DMSO of the corresponding compound in cell culture. Afterward, the intermediate dilutions of the compounds were serially diluted to the appropriate concentration (ranging from 0 to 10 µM) and the cells were incubated for another 24 h (0.6% (v/v) is the maximum final content of DMSO). DMSO at comparable concentrations did not show any effects on cell cytotoxicity. Cytotoxicity was determined using a MTT assay (MTT, 3-(4,5- dimethyl 2-thiazolyl)-2,5-diphenyl-2H-tetrazolium bromide). MTT (0.1 mg ml^{-1} solution) was added to the cells and the plates were further incubated for 3 h. Then the culture medium was removed and the purple formazan crystals formed by the mitochondrial dehydrogenase and reductase activity of vital cells were dissolved in DMSO. The optical density, directly proportional to the number of surviving cells, was quantified at 570 nm (background correction at 620 nm) using a multiwell plate reader Multiskan FC and the fraction of surviving cells was calculated from the absorbance of untreated control cells. The Inhibitory Concentration 50 (IC_{50}) value indicates the concentration needed to inhibit the biological function of the cells by half and is presented as the mean (± standard error (SD)) of three independent experiments, each comprising three microcultures per concentration level.

Trypan Blue assay. To ensure cellular viability of PBMC and U937, the trypan blue (TB) exclusion assay was carried out. It has been established that cell membrane integrity is a basic criterion for distinguishing dead from live cells. The TB method is a very common assay for evaluating cytotoxicity in experimental investigations where dead cells absorb TB into the cytoplasm because of membrane integrity loss, whereas live cells remain unstained [38]. Thus, the relative number of live cells is obtained by optical microscopy by counting the number of unstained (live) cells using the Thoma chamber.

2.3.3 Flow cytometric detection of cell death

To perform the ANX/7AAD test [39, 40], cells were resuspended in 200 µl of 1x binding buffer (Clonetech Laboratories), and stained with 5 µl of AnxV FITC-conjugated for 10 min. Staining and analysis were performed following the manufacturer's instructions. Then, 7-AAD (7-amino-actino-mycin D, Molecular Probes) were added to obtain a final concentration of 1µg/ml. For simultaneous detection of 7-AAD and Annexin V staining, non-permeabilized cells were incubated for 20 min at room temperature in the dark. 7-AAD+ events were calculated as percentage of total events and considered as late apoptotic/necrotic cells. For each experimental condition, at least 10,000 total events were collected.

2.3.4 Determination of Mitochondria and Mitochondrial Reactive Oxygen Species (ROS)

For mitochondria detection, cells were stained with 100 nM MitoTracker red (MTR, Molecular Probes, Italy) and incubated for 30 min as previously reported [41]. MTR passively diffuses across the plasma membrane of live cells and accumulates in active mitochondria. The MitoTracker series exhibit reliable retention in mitochondria and are able to track mitochondrial morphology even after cell death, fixation and permeabilization. Due to this unique property, they were preferred in many specialized research areas [42]. MitoSOX Red (Thermo Fisher Scientific, Waltham, MA, USA) is a fluorigenic dye specifically targeted to mitochondria in live cells. Oxidation of this probe by superoxide that is contained in the mitochondria produces a red fluorescence. MitoSOX Red, 5 µM, was added to the samples 10 min before the time of acquisition. The samples were analyzed by flow cytometry using the appropriate fluorescence channel [43].

2.3.5 Autophagosome Detection

After the treatment with dendrimers, cells were incubated with 50 µM monodansylcadaverine (MDC, Sigma-Aldrich) at 37 °C for 10 min and then analyzed by flow cytometry. MDC is an autofluorescent dye that accumulates in autophagic-involved vacuoles (AIVs) due to a combination of ion trapping and specific interactions with membrane lipids.

2.3.6 Monoclonal Antibodies

The monoclonal antibodies (MAbs) for flow cytometry used in this work were anti-CD3 APC (clone UCHT1, Biolegend, San Diego, California, USA) and anti-CD11b APC (clone M1/70, BD Biosciences, San Jose, California, USA). For the CD11b detection, cells were harvested and washed with PBS. Then, cells were incubated with direct fluorescein isothiocyanate-labeled anti-CD11b antibody (BD Biosciences) in the dark. After 20 mins, cells were washed with PBS and detected by flow cytometry.

2.3.7 Flow Cytometry Assays

The cytometric experiments were carried out with a FACSCanto II flow cytometer (BD, Franklin Lakes, NJ, USA) equipped with an argon laser (Blue, Ex 488 nm), a helium–neon laser (Red, Ex 633 nm), and a solid-state diode laser (Violet, Ex 405 nm). The analyses were performed with FACSDivaTM software (version 4.1.1, BD, Franklin Lakes, NJ, USA); approximately 10,000 cell events were acquired for each sample.

2.3.8 Confocal Microscopy Analyses

Confocal microscopy analyses were performed by a Leica TCS SP5 II confocal microscope (Leica Microsystem, Wetzlar, Germany) with 488, 543, and 633 nm illuminations and oil-immersed objectives. For confocal live imaging, the cells were grown on MatTek glass bottom chambers (MatTek Corporation, Bratislava, Slovak Republic). The images were further processed and analyzed in ImageJ software (version 1.34e, NIH, Bethesda, MD, USA).

Acknowledgements: This work was supported by grants from CTQ2017-86224-P (MINECO), Consortium IMMUNOTHERCAN-CM B2017/BMD-3733 (CAM), project SBPLY/17/180501/000358 JCCM and the Comunidad de Madrid Research Talent Attraction Program 2017-T2/IND-5243. CIBER-BBN is an initiative funded by the VI National R&D&i Plan 2008–2011, Iniciativa Ingenio 2010, Consolider Program, CIBER Actions and financed by the Instituto de Salud Carlos III with assistance from the European Regional Development

Fund. N. S.O. wishes to thank JCCM for a predoctoral fellowship. This work has been supported partially by a EUROPARTNER: Strengthening and spreading international partnership activities of the Faculty of Biology and Environmental Protection for interdisciplinary research and innovation of the University of Lodz Program: NAWA International Academic Partnership Program. This article/publication is based upon work from COST Action CA 17140 "Cancer Nanomedicine from the Bench to the Bedside" supported by COST (European Cooperation in Science and Technology). We thank Sarah Tassinari for the help with the EPR experiments and Caterina Ciacci for the confocal microscope images.

Conflicts of Interest: The authors declare no conflict of interest. The funders had no role in the design of the study; in the collection, analyses, or interpretation of data; in the writing of the manuscript, or in the decision to publish the results.

Highlights

- Ring-substituted iminopyridine Cu(II)-metallodendrimers were synthesized.
- The metallodendrimers exhibited potent activity as antitumor agents.
- Iminopyridine substitution produced an increased cytotoxicity in tumor cells.
- Selective cytotoxicity towards U937 tumor cells, while PBMC are barely affected.
- Outstanding ROS production in U937 cells with the pair Me/Cl and OMe/NO_3.

TOC graphic

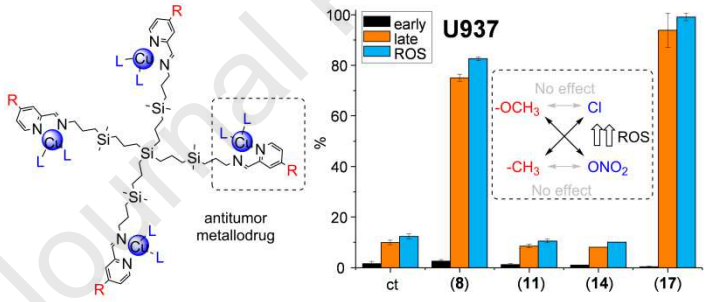

References

[1] R.L. Siegel, K.D. Miller, A. Jemal, Cancer statistics, 2020, CA: A Cancer J. Clin., 70 (2020) 7-30.

[2] T.N. Seyfried, L.C. Huysentruyt, On the origin of cancer metastasis, Crit. Rev. Oncog., 18 (2013) 43-73.

[3] A. Aghebati-Maleki, S. Dolati, M. Ahmadi, A. Baghbanzhadeh, M. Asadi, A. Fotouhi, M. Yousefi, L. Aghebati-Maleki, Nanoparticles and cancer therapy: Perspectives for application of nanoparticles in the treatment of cancers, J. Cell. Physiol., 235 (2020) 1962-1972.

[4] H. Chen, Z. Zhen, T. Todd, P.K. Chu, J. Xie, Nanoparticles for improving cancer diagnosis, Mater. Sci. Eng. R Rep., 74 (2013) 35-69.

[5] T. Boulikas, M. Vougiouka, Recent clinical trials using cisplatin, carboplatin and their combination chemotherapy drugs (review), Oncol. Rep., 11 (2004) 559-595.

[6] D.-W. Shen, L.M. Pouliot, M.D. Hall, M.M. Gottesman, Cisplatin resistance: a cellular self-defense mechanism resulting from multiple epigenetic and genetic changes, Pharmacol. Rev., 64 (2012) 706-721.

[7] K. Gałczyńska, Z. Drulis-Kawa, M. Arabski, Antitumor activity of Pt(II), Ru(III) and Cu(II) complexes, Molecules, 25 (2020) 3492.

[8] N. Sanz del Olmo, R. Carloni, P. Ortega, S. García-Gallego, F.J. de la Mata, Chapter One - Metallodendrimers as a promising tool in the biomedical field: An overview, in: P.J. Pérez (Ed.) Adv. Organomet. Chem., Academic Press, 2020, pp. 1-52.

[9] B. Canonico, R. Carloni, N. Sanz del Olmo, S. Papa, M.G. Nasoni, A. Fattori, M. Cangiotti, F.J. de la Mata, M.F. Ottaviani, S. García-Gallego, Fine-tuning the interaction and therapeutic effect of Cu(II) carbosilane metallodendrimers in cancer cells: An in vitro Electron Paramagnetic Resonance study, Mol. Pharm., 17 (2020) 2691-2702.

[10] R. Carloni, N. Sanz Del Olmo, P. Ortega, A. Fattori, R. Gómez, M.F. Ottaviani, S. García-Gallego, M. Cangiotti, F.J. de la Mata, Exploring the interactions of ruthenium (II) carbosilane metallodendrimers and precursors with model cell membranes through a dual spin-label spin-probe technique using EPR, Biomolecules, 9 (2019).

[11] K. Kumar, Quantitative structure activity relationship in drug design: An overview, SF J. Pharm. Anal. Chem., 2 (2019) 1017(1011-1013).

[12] K. Dankhoff, M. Gold, L. Kober, F. Schmitt, L. Pfeifer, A. Dürrmann, H. Kostrhunova, M. Rothemund, V. Brabec, R. Schobert, B. Weber, Copper(II) complexes with tridentate Schiff base-like ligands: solid state and solution structures and anticancer activity, Dalton Trans., 48 (2019) 15220-15230.

[13] P.N. Craig, Interdependence between physical parameters and selection of substituent groups for correlation studies, J. Med. Chem., 14 (1971) 680-684.

[14] N. Sanz del Olmo, R. Carloni, A.M. Bajo, P. Ortega, A. Fattori, R. Gómez, M.F. Ottaviani, S. García-Gallego, M. Cangiotti, F.J. de la Mata, Insight into the antitumor activity of carbosilane Cu(ii)–metallodendrimers through their interaction with biological membrane models, Nanoscale, 11 (2019) 13330-13342.

[15] M. Maroto-Díaz, B.T. Elie, P. Gómez-Sal, J. Pérez-Serrano, R. Gómez, M. Contel, F. Javier de la Mata, Synthesis and anticancer activity of carbosilane metallodendrimers based on arene ruthenium(II) complexes, Dalton Trans., 45 (2016) 7049-7066.

[16] J.F. Bermejo, P. Ortega, L. Chonco, R. Eritja, R. Samaniego, M. Müllner, E. de Jesus, F.J. de la Mata, J.C. Flores, R. Gomez, A. Muñoz-Fernandez, Water-soluble carbosilane dendrimers: Synthesis, biocompatibility and complexation with oligonucleotides; evaluation for medical applications, Chem. Eur. J. , 13 (2007) 483-495.

[17] N. Sanz del Olmo, M. Maroto-Díaz, R. Gómez, P. Ortega, M. Cangiotti, M.F. Ottaviani, F.J. de la Mata, Carbosilane metallodendrimers based on copper (II) complexes: Synthesis, EPR characterization and anticancer activity, J. Inorg. Biochem., 177 (2017) 211-218.

[18] D.E. Budil, S. Lee, S. Saxena, J.H. Freed, Nonlinear-Least-Squares analysis of slow-motion EPR spectra in one and two dimensions using a modified Levenberg–Marquardt algorithm, J. Magn. Reson., 120 (1996) 155-189.

[19] E. Garribba, G. Micera, The determination of the geometry of Cu(II) complexes: An EPR spectroscopy experiment, J. Chem. Educ., 83 (2006) 1229.

[20] M.F. Ottaviani, N. El Brahmi, M. Cangiotti, C. Coppola, F. Buccella, T. Cresteil, S. Mignani, A.M. Caminade, J.P. Costes, J.P. Majoral, Comparative EPR studies of Cu(ii)-conjugated phosphorous-dendrimers in the absence and presence of normal and cancer cells, RSC Adv., 4 (2014) 36573-36583.

[21] M.F. Ottaviani, M. Cangiotti, A. Fattori, C. Coppola, S. Lucchi, M. Ficker, J.F. Petersen, J.B. Christensen, Copper(II) complexes with 4-carbomethoxypyrrolidone functionalized PAMAM-dendrimers: an EPR study, J. Phys. Chem. B, 117 (2013) 14163-14172.

[22] M.F. Ottaviani, S. Bossmann, N.J. Turro, D.A. Tomalia, Characterization of starburst dendrimers by the EPR technique. 1. Copper complexes in water solution, J. Am. Chem. Soc., 116 (1994) 661-671.

[23] Y.-H. Tang, M. Cangiotti, C.-L. Kao, M.F. Ottaviani, EPR characterization of copper(II) complexes of PAMAM-Py dendrimers for biocatalysis in the absence and presence of reducing agents and a spin trap, J. Phys. Chem. B, 121 (2017) 10498-10507.

[24] M. Altaf, M. Monim-ul-Mehboob, A.A.A. Seliman, M. Sohail, M.I.M. Wazeer, A.A. Isab, L. Li, V. Dhuna, G. Bhatia, K. Dhuna, Synthesis, characterization and anticancer activity of gold(I) complexes that contain tri-tert-butylphosphine and dialkyl dithiocarbamate ligands, European Journal of Medicinal Chemistry, 95 (2015) 464-472.

[25] N. Sanz del Olmo, A.M. Bajo, M. Ionov, S. García-Gallego, M. Bryszewska, R. Gómez, P. Ortega, F.J. de la Mata, Cyclopentadienyl ruthenium(II) carbosilane metallodendrimers as a promising treatment against advanced prostate cancer, European Journal of Medicinal Chemistry, 199 (2020) 112414.

[26] K. Zubčić, V. Radovanović, J. Vlainić, P.R. Hof, N. Oršolić, G. Šimić, M. Jazvinšćak Jembrek, PI3K/Akt and ERK1/2 Signalling Are Involved in Quercetin-Mediated Neuroprotection against Copper-Induced Injury, Oxidative Medicine and Cellular Longevity, 2020 (2020) 9834742.

[27] X. Li, S. Hao, A. Han, Y. Yang, G. Fang, J. Liu, S. Wang, Intracellular Fenton reaction based on mitochondria-targeted copper(ii)–peptide complex for induced apoptosis, J. Mater. Chem. B, 7 (2019) 4008-4016.

[28] C. Saporito-Magriñá, R. Musacco-Sebio, J.M. Acosta, S. Bajicoff, P. Paredes-Fleitas, S. Reynoso, A. Boveris, M.G. Repetto, Copper(II) and iron(III) ions inhibit respiration and increase free radical-mediated phospholipid peroxidation in rat liver mitochondria: Effect of antioxidants, Journal of Inorganic Biochemistry, 172 (2017) 94-99.

[29] I.J. Chen, R. Taneja, D. Yin, P.R. Seo, D. Young, A.D. MacKerell, Jr., J.E. Polli, Chemical substituent effect on pyridine permeability and mechanistic insight from computational molecular descriptors, Mol. Pharm., 3 (2006) 745-755.

[30] N. Guo, M. Azadniv, M. Coppage, M. Nemer, J. Mendler, M. Becker, J. Liesveld, Effects of neddylation and mTOR inhibition in acute myelogenous leukemia, Transl. Oncol., 12 (2019) 602-613.

[31] Y. Matsuzawa-Ishimoto, S. Hwang, K. Cadwell, Autophagy and Inflammation, Annu. Rev. Immunol., 36 (2018) 73-101.

[32] A. Onnis, C. Cassioli, F. Finetti, C.T. Baldari, Regulation of selective B cell autophagy by the pro-oxidant adaptor p66SHC, Front. Cell Dev. Biol., 8 (2020).

[33] K.L. Conway, P. Kuballa, B. Khor, M. Zhang, H.N. Shi, H.W. Virgin, R.J. Xavier, ATG5 regulates plasma cell differentiation, Autophagy, 9 (2013) 528-537.

[34] N. Germic, Z. Frangez, S. Yousefi, H.-U. Simon, Regulation of the innate immune system by autophagy: neutrophils, eosinophils, mast cells, NK cells, Cell Death Differ., 26 (2019) 703-714.

[35] C. Li, E. Capan, Y. Zhao, J. Zhao, D. Stolz, S.C. Watkins, S. Jin, B. Lu, Autophagy is induced in CD4+ T cells and important for the growth factor-withdrawal cell death, J. Immunol., 177 (2006) 5163-5168.

[36] L. Adamo, C. Rocha-Resende, D.L. Mann, The emerging role of B lymphocytes in cardiovascular disease, Annu. Rev. Immunol., 38 (2020) 99-121.

[37] I. Prager, C. Liesche, H. van Ooijen, D. Urlaub, Q. Verron, N. Sandström, F. Fasbender, M. Claus, R. Eils, J. Beaudouin, B. Önfelt, C. Watzl, NK cells switch from granzyme B to death receptor-mediated cytotoxicity during serial killing, J. Exp. Med., 216 (2019) 2113-2127.

[38] B.A. Avelar-Freitas, V.G. Almeida, M.C. Pinto, F.A. Mourão, A.R. Massensini, O.A. Martins-Filho, E. Rocha-Vieira, G.E. Brito-Melo, Trypan blue exclusion assay by flow cytometry, Braz. J. Med. Biol. Res., 47 (2014) 307-315.

[39] B. Canonico, M. Betti, F. Luchetti, M. Battistelli, E. Falcieri, P. Ferri, L. Zamai, D. Barnett, S. Papa, Flow cytometric profiles, biomolecular and morphological aspects of transfixed leukocytes and red cells, Cytometry B Clin. Cytom., 78 (2010) 267-278.

[40] M. Betti, A. Minelli, B. Canonico, P. Castaldo, S. Magi, M.C. Aisa, M. Piroddi, V. Di Tomaso, F. Galli, Antiproliferative effects of tocopherols (vitamin E) on murine glioma C6 cells: homologue-specific control of PKC/ERK and cyclin signaling, Free Radic. Biol. Med., 41 (2006) 464-472.

[41] F. Luchetti, B. Canonico, E. Cesarini, M. Betti, L. Galluzzi, L. Galli, J. Tippins, C. Zerbinati, S. Papa, L. Iuliano, 7-Ketocholesterol and 5,6-secosterol induce human endothelial cell dysfunction by differential mechanisms, Steroids, 99 (2015) 204-211.

[42] X. Zhang, Q. Sun, Z. Huang, L. Huang, Y. Xiao, Immobilizable fluorescent probes for monitoring the mitochondria microenvironment: a next step from the classic, J. Mater. Chem. B, 7 (2019) 2749-2758.

[43] B. Canonico, G. Di Sario, E. Cesarini, R. Campana, F. Luchetti, L. Zamai, C. Ortolani, M.G. Nasoni, W. Baffone, S. Papa, Monocyte response to different Campylobacter jejuni lysates involves endoplasmic reticulum stress and the lysosomal¯mitochondrial axis: When cell death is better than cell survival, Toxins, 10 (2018).

Elaborated study of Cu(II) carbosilane metallodendrimers bearing substituted iminopyridine moieties as antitumor agents

Riccardo Carloni [1], Natalia Sanz del Olmo [2], Barbara Canonico [3], Mariele Montanari [3], Caterina Ciacci [3], Gianluca Ambrosi [1], F. Javier de la Mata [2,4,5*], Maria Francesca Ottaviani [1*], and Sandra García-Gallego [2,4,5*]

[1] Department of Pure and Applied Sciences, University of Urbino "Carlo Bo", 61029, Urbino, Italy
[2] Department of Organic and Inorganic Chemistry, and Research Institute in Chemistry "Andrés M. del Río" (IQAR), University of Alcalá, 28805, Madrid, Spain
[3] Department of Biomolecular Science (DiSB), University of Urbino "Carlo Bo", Urbino 61029, Italy
[4] Networking Research Center on Bioengineering, Biomaterials and Nanomedicine (CIBER-BBN), 28029, Madrid, Spain
[5] Institute Ramón y Cajal for Health Research (IRYCIS), 28034, Madrid, Spain
* Correspondence: sandra.garciagallego@uah.es, javier.delamata@uah.es, maria.ottaviani@uniurb.it

Highlights

- Ring-substituted iminopyridine Cu(II)-metallodendrimers were synthesized.
- The metallodendrimers exhibited potent activity as antitumor agents.
- Iminopyridine substitution produced an increased cytotoxicity in tumor cells.
- Selective cytotoxicity towards U937 tumor cells, while PBMC are barely affected.
- Outstanding ROS production in U937 cells with the pair Me/Cl and OMe/NO_3.

Declaration of interests

☒ The authors declare that they have no known competing financial interests or personal relationships that could have appeared to influence the work reported in this paper.

☐The authors declare the following financial interests/personal relationships which may be considered as potential competing interests: